(2)

AD-A222 682

DTIC ELECTE JUN 13 1990 S D

UMENTATION PAGE

Form Approved OMB No. 0704-0188

U	1b. RESTRICTIVE MARKINGS: NA
2a. SECURITY CLASSIFICATION AU[illegible]TY: NA	3. DISTRIBUTION/AVAILABILITY OF REPORT: Unlimited
2b. DECLASSIFICATION/DOWNGRA[illegible]G SCHEDULE: NA	
4. PERFORMING ORGANIZATION [illegible]RT NUMBER(S): NA	5. MONITORING ORGANIZATION REPORT NUMBER(S): NA
6a. NAME OF PERFORMING ORGANIZATION: Oregon State University	6b. OFFICE SYMBOL (If applicable): NA
6c. ADDRESS (City, State, and ZIP Code): Corvallis, Oregon 97331-6503	7a. NAME OF MONITORING ORGANIZATION: Office of Naval Research
	7b. ADDRESS (City, State, and ZIP Code): 800 N. Quincy Street Arlington, Virginia 22217-5000
8a. NAME OF FUNDING/SPONSORING ORGANIZATION: Office of Naval Research	8b. OFFICE SYMBOL (If applicable): ONR
	9. PROCUREMENT INSTRUMENT IDENTIFICATION NUMBER: N00014-88-K-0388
8c. ADDRESS (City, State, and ZIP Code): 800 N. Quincy Street Arlington, Virginia 22217-5000	10. SOURCE OF FUNDING NUMBERS: PROGRAM ELEMENT NO. / PROJECT NO. / TASK NO. / WORK UNIT ACCESSION NO.

11. TITLE (Include Security Classification)

(U) DNA-mediated electron transfer and application to 'biochip' development

12. PERSONAL AUTHOR(S)
Ho, Pui S.

13a. TYPE OF REPORT	13b. TIME COVERED	14. DATE OF REPORT (Year, Month, Day)	15. PAGE COUNT
Annual	FROM 6/89 TO 5/90	90/5/30	9

16. SUPPLEMENTARY NOTATION
NA

17. COSATI CODES		
FIELD	GROUP	SUB-GROUP

18. SUBJECT TERMS (Continue on reverse if necessary and identify by block number)
Electron transfer, biochips, DNA, Biochemistry, Quenching, Single Crystals (JG)

19. ABSTRACT (Continue on reverse if necessary and identify by block number)

We are studying the electronic properties of DNA to determine the applicability of this molecule to the design and microelectronic components. The properties of interest include the electronic coupling between stacked bases and their effects on conductance of DNA double helices. Single crystal polarized reflectance spectroscopy and photoflash kinetic methods are used for these studies.

DISTRIBUTION STATEMENT A
Approved for public release;
Distribution Unlimited

20. DISTRIBUTION/AVAILABILITY OF ABSTRACT	21. ABSTRACT SECURITY CLASSIFICATION
☒ UNCLASSIFIED/UNLIMITED ☐ SAME AS RPT. ☐ DTIC USERS	(U)
22a. NAME OF RESPONSIBLE INDIVIDUAL: Michael Marron	22b. TELEPHONE (Include Area Code): (206) 696-4760 / 22c. OFFICE SYMBOL

DD Form 1473, JUN 86 — Previous editions are obsolete. — SECURITY CLASSIFICATION OF THIS PAGE

S/N 0102-LF-014-6603

9

Date: May 30, 1990

Annual Report on Cr act N00014-88-K-0388 R&T Code 441N046

Principal Investigator: Pui Shing Ho

Contractor: Oregon State University
Contract Title: DNA mediated electron transfer and application to 'Biochip' development

Contract Period: 1988 June 1 through 1991 May 31

Research objective: The application of biological molecules for fabrication of advanced electronic components requires detailed data on the electronic properties of these molecules. This project focuses on the conductance properties of double stranded DNA molecules to determine the suitability of these molecules for this purpose.

Progress (Year 2): In terms of understanding the electronic properties of double stranded DNA, we have (in collaboration with Professor Leigh B. Clark, in the Department of Chemistry at the University of California in San Diego) studied the polarized reflectance spectra of single crystals of Z-DNA. Hexamer DNA sequences that crystallize as Z-DNA have crystal packings that align each half turn of the Z-DNA duplex end-to-end to form essentially continuous strands of DNA. The bases are all aligned perpendicular to the crystallographic c-axis, thus allowing us to study the in-plane and out-of-plane electronic transitions of a known structure. From these studies, we concluded that the hyperchromism UV absorption at 295 nm and concommitant hypochromism at 260 nm of Z- versus B-DNA results from a red shift of an in-plane π-π^* transition rather than an out-of-plane n-π^* transition. The extent of hypochromism of the entire UV spectrum was explained using a point-dipole interaction model for a polymer of infinite length (see enclosed preprint).

We further gained an understanding of through bond electronic interactions between fluorescent probes and nitroxide spin labels in a study (in collaboration with Dr. Neil V. Blough in the Department of Chemistry at the Woods Hole Oceanographic Institute) that measures the fluorescence quenching by nitroxyl radicals. In this study, a series of nitroxide-fluorophore adducts were synthesized and their rate of fluorescence decay measured over time. These studies showed that the quenching mechanism arises through electron exchange which causes relaxation of the excited

singlet state to the triplet and/or ground state of the fluorophore (see enclosed preprint).

The studies designed to measure the rate of electron transfer directly through double stranded DNA were beset by electronic problems in the instrumentation. The transient data recorder of computer interface for the flash photolysis apparatus arrived defective. This piece of equipment was just recently repaired and returned to us and we are currently testing the new configuration.

Work Plan (Year 3): In the second year, we plan to complete the assembly and testing of the flash photolysis apparatus and programs. Once this is complete, we will begin the studies to measure the length dependence of electron transfer reactions through the DNA oligomers. Meanwhile, we have designed a set of steady-state experiments in which a metal free porphyrin will be intercalated to the d(CG) end of a polymer, and an Fe(III) porphyrin bound to the minor groove of the d(TA) end. The accumulation of photoreduced Fe(III) porphyrin will be monitored as a function of time for a continuous excitation source. From the concentration dependence for the reduction rate, we can determine the intramolecular electron transfer rate constant for electron conductance throught the DNA. By varying the length of the intervening sequences we can determine the length dependence of these rates. The DNA polymers and porphyrins have been synthesized for these studies. These studies do not relie on the flash photolysis apparatus that has been giving us problems.

We further plan to measure the polarized single crystal reflectance spectra of different DNA sequences in their B- and Z- conformations to study the sequence and conformation dependence of the electronic coupling between the bases of double helical DNA.

Inventions: None

Publications:

1. 'Polarized Electronic Spectra of Z-DNA Single Crystals', Ho, P.S., Zhou, G., and Clark, L.B., Biopolymers, in press.

2. 'Intramolecular Quenching of Excited Singlet States by Stable Nitroxyl Radicals', Green, S.A., Simpson, D.J., Zhou, G., Ho, P.S., and Blough, N.V., J. Am. Chem. Soc., in press.

Training activities: There are currently two graduate students working on this project and we have had three undergraduates working intermittantly on

the synthesis phases of the project. The two graduate students are Mr. Guangwen Zhou, a third year Ph.D. candidate, and Mr. Todd F. Kagawa, a second year Ph.D. candidate. Mr. Zhou, a citizen of the People's Republic of China, has a good background in physics and has already made remarkable progress towards his degree. Mr. Kagawa, a citizen of the U.S.A., is strong in chemical synthesis and purification techniques. A third graduate student, Mr. Bernhard Geierstranger, is completing his Masters of Science degree this July and is entering a Ph.D. program in the Department of Biophysics at the University of California at Berkeley this fall.

The demographic data you have requested regarding these students are:

Women and minorities: 0

Non-citizens: 2 (Peoples Republic of China and Federal Republic of Germany)

Awards/Fellowships: None

REVISED VERSION SUBMITTED 5/9/90

Intramolecular Quenching of Excited Singlet States by Stable Nitroxyl Radicals

S. A. Green,[•] D. J. Simpson,[#] G. Zhou,[+] P. S. Ho,[+] and N. V. Blough[•*]

[•]Department of Chemistry
Woods Hole Oceanographic Institution
Woods Hole, Massachusetts 02543

[+]Department of Biochemistry and Biophysics
Oregon State University, Corvalis, Oregon 97331

[#]Present address: Life Sciences Division
Los Alamos National Laboratory
Los Alamos, New Mexico 87545

*To Whom Correspondence Should be Addressed

ABSTRACT

Absorbance and steady-state and time-resolved fluorescence measurements were employed to examine the mechanism(s) of excited singlet state quenching by nitroxides in a series of nitroxide-fluorophore adducts. This work establishes the following: 1) the absorption and emission energies of the fluorophores are unaffected by the presence of the nitroxide substituent(s), and the residual emission that is observed from the adducts arises from the locally excited singlet of the fluorophore, not from charge recombination; 2) rate constants for intramolecular quenching by the nitroxides (k_q) are high (10^8 -10^{10} s^{-1}) and decrease significantly with increasing nitroxide to fluorophore distance - however, relatively high rates of quenching (>10^8 s^{-1}) are observed over distances as great as 12 Å; 3) Förster energy transfer does not contribute significantly to the quenching due to the low values for the spectral overlap integrals; 4) the k_q's do not increase proportionally to the solvent-dependent increases in the Dexter overlap integral, indicating that energy transfer by the Dexter mechanism is not responsible for the quenching; 5) the values of k_q show no obvious correlation with the calculated free energies for photo-induced electron transfer, suggesting that this quenching pathway is also unimportant; 6) for hematoporphyrin-nitroxide adducts, which contain a fluorophore whose singlet energy is below that of the first excited state energy of the nitroxide (thus precluding energy transfer), significant rates of quenching are still observed; 7) for compounds with similar nitroxide-fluorophore distances, an approximately linear correlation is observed between the k_q's of the paramagnetic compounds and the non-radiative rate constants of the diamagnetic reference compounds, suggesting that the nitroxide moiety catalyses a pre-existing non-radiative pathway in the fluorophore. These results indicate that the quenching arises through electron exchange which causes relaxation of the (local) singlet state to the triplet and/or ground state of the fluorophore.

Introduction

Diffusional quenching by stable nitroxyl radicals of excited singlet[1], doublet [2] and triplet[1d,f,3-10] states and of excimers [11] has been studied extensively over the past twenty years. The goal of much of this work has been to understand the mechanism(s) through which excited states are quenched by paramagnetic species. Recently however, fluorescence quenching by nitroxides has also become an important tool with which to probe the structural and dynamical properties of membranes[12] and micelles.[13]

While it has been generally accepted that nitroxide quenching of singlet states can result from an electron exchange-induced[14] intersystem crossing to the triplet[1b,e] or internal conversion to the ground state,[1e-g] significant contributions to the quenching may also arise from charge[1f] and/or energy transfer.[1a,12d] Green et al.[1b] argued that charge (electron) transfer is unimportant owing to a lack of solvent dependence of the quenching rate constant. However, as noted by Chattopadhyay et al.,[1f] the quenching occurs at the diffusion limit and thus may not be differentiated by solvent polarity.[15] Green et al.[1b] also suggested that Förster energy transfer[16] is insignificant because of the low extinction coefficients of the nitroxides in the 400-550 nm spectral region. Recent work by Puskin et al.[12d] suggests that energy transfer can be important and, in some cases, can extend the quenching radius to as much as 10 Å, approximately twice the interaction distance originally calculated by Green et al.[1b] Furthermore, energy transfer by electron exchange[17] cannot be excluded a priori for compounds having singlet energies greater than the lowest excited state energy of the nitroxide (~2.6 eV for the piperidinyl nitroxides).

Until recently, information on the efficiency of intramolecular quenching of excited states by nitroxides was unavailable. We have shown that intramolecular quenching of excited singlets is highly efficient,[18] and that covalently linked, nitroxide-fluorophore adducts can be employed as very sensitive optical probes of radical/redox reactions.[18-21] These adducts also offer a means of studying the mechanism(s) of nitroxide quenching in more detail and of establishing the distance dependence and possible importance of "through-bond"[15] vs "through-

space" interactions in the quenching. This information is essential for the construction of better optical radical sensors,[18-20] for a more complete analysis of nitroxide quenching in biophysical studies[12,13] and for an understanding of the possible influence of stable or transient radicals on excited states in biological and chemical systems.

In this study, we examine the photophysical properties of a number of nitroxide-fluorophore adducts and their diamagnetic analogues. By employing compounds having fluorophores with differing singlet energies and a range of nitroxide-fluorophore distances, we attempt to assess the relative contributions of energy transfer, electron transfer, and electron exchange-induced relaxation to the intramolecular quenching of singlet states by nitroxides.

Results and Discussion

A. Absorption, Excitation, and Emission Spectra

Table 1 summarizes the absorption and emission energies of I-IV (Fig. 1) in various solvents. In water, methanol, acetonitrile, dioxane and hexane, the absorption spectra of the nitroxide-fluorophore adducts were indistinguishable from the sum of the individual spectral contributions of the fluorophore and nitroxide substituents. Other than the loss of the weak nitroxide contribution in the visible (430-480 nm, $\varepsilon \approx 10\text{-}13\ M^{-1}cm^{-1}$) and ultraviolet (~246 nm, $\varepsilon \approx 2x10^3\ M^{-1}cm^{-1}$), the spectra of the O-acetyl and methyl ester derivatives (Fig. 1) were identical to those of the corresponding nitroxides. No evidence for optical charge transfer bands or enhanced ground to triplet absorption[14] by the fluorophore could be found in the spectra of the nitroxide adducts. While the absorption spectra of the fluorophores were largely insensitive to solvent polarity, the lowest energy band ($n\text{-}\pi^*$) of the nitroxides[22] shifted substantially to the blue with increasing solvent polarity as previously noted.[23] The influence of this shift on singlet state quenching will be addressed below (Section D).

The fluorescence excitation spectra of the nitroxide adducts matched the absorption spectra of the fluorophore substituents and were indistinguishable from the excitation spectra of the corresponding diamagnetic derivatives.

The lineshapes of the emission spectra were identical for the nitroxide adducts and the corresponding diamagnetic derivatives, and generally showed a mirror-image relationship to the excitation spectra (Fig. 2). With increasing solvent polarity, identical red-shifts in the emission maxima were observed for the nitroxide and diamagnetic adducts of a given substitution. These results indicate that the residual emission from the nitroxide adducts is arising from the same locally excited singlet state of the fluorophore substituent as in the diamagnetic derivatives and is not produced through charge recombination.[24] No evidence for exciplex emission from the paramagnetic adducts could be found in either polar (acetonitrile) or nonpolar (hexane) solvents.

B. Quantum Yield and Lifetime Measurements

While the presence of the nitroxyl radical substituent(s) did not influence the absorption and emission energies of the fluorophores in the adducts, the fluorescence quantum yields and lifetimes of the nitroxide adducts were reduced substantially relative to their corresponding diamagnetic derivatives in both polar and nonpolar solvents (Table 2, Fig. 3). The fluorescence decay of the nitroxide adducts could be well fit to a sum of two exponentials but was dominated by the short-lived component (Fig. 3). The small, long-lived component usually represented $\leq$5% of the total amplitude. We attribute this component to minor diamagnetic contaminants, based on assessments of compound purity.

With few exceptions, the fluorescence decay of the diamagnetic derivatives could be fit as a single exponential process (Fig. 3). The O-acetyl and methyl ester derivatives of a given substitution showed very similar lifetimes and quantum yields (Table 2). These results indicate that the rate constants for radiative and non-radiative decay of the singlet do not differ significantly between the O-acetyl and the methyl ester derivatives (Fig. 1). This leads us to conclude that, unlike the situation for aliphatic and aromatic amines,[25] intramolecular quenching (via electron transfer) by the hindered, O-substituted hydroxylamines is unimportant. Preliminary work on other O-substituted hydroxylamines is consistent with this conclusion.[19] In contrast, the unsubstituted hydroxylamine does appear to quench partially.[19,26]

The steady-state and time-resolved fluorescence measurements of the paramagnetic and diamagnetic forms can be related by

(1) $$\phi_d = \frac{k_r}{k_r + k_{nr}}, \qquad k_r + k_{nr} = \frac{1}{\tau_d}$$

(2) $$\phi_p = \frac{k_r}{k_r + k_{nr} + k_q}, \qquad k_r + k_{nr} + k_q = \frac{1}{\tau_p}$$

where ϕ_d (ϕ_p) and τ_d (τ_p) are the quantum yields and lifetimes of the diamagnetic (paramagnetic) compounds, respectively, k_r and k_{nr} are the rate constants for radiative and non-radiative decay of the diamagnetic compounds, and k_q is the intramolecular (non-radiative) quenching rate constant attributable to the nitroxide moiety. If k_r and k_{nr} are unaltered by the presence of the nitroxide, then

(3) $$\frac{\phi_d}{\phi_p} = \frac{\tau_d}{\tau_p}$$

(4) $$k_q = \frac{1}{\tau_p} - \frac{1}{\tau_d}$$

The measured ratios τ_d/τ_p and ϕ_d/ϕ_p are equal within the uncertainties (Table 2), indicating that this condition applies. Errors are largest in the determination of ϕ_p since traces of highly fluorescent impurities can produce significant overestimates of such low quantum yields, leading to low ϕ_d/ϕ_p ratios. For this reason, rate constants for intramolecular quenching, k_q (Table 3) were calculated from the lifetime data employing Eqn. 4, except in the case of compound IA where lifetimes were too short to be resolved by the instrument. For this compound the expected lifetimes were computed from Eqn. 3 using the quantum yield data and the lifetime of the diamagnetic O-acetyl (IB). Lifetime data show <3% of a long-lived component for IA.[27]

In aprotic solvents such as acetonitrile and hexane, k_q increased from $\approx 10^8$ s^{-1} to 10^{10} s^{-1} in the order ID < IIA < IIIA < IVA < IA. This sequence reflects not only the

differences in nitroxide-fluorophore distance but also the type, number and position of the naphthalene-nitroxide linkage(s) (vide infra). With the exception of compounds IA and ID, no significant differences were observed between k_q's measured in polar (acetonitrile) and nonpolar (hexane) solvents. Surprisingly, the k_q's for compounds IA and ID actually increased slightly with decreasing solvent polarity (Table 3).

C. Dependence of k_q on Distance, Linkage Position and Type

Because the distance and orientation of the nitroxide with respect to the fluorophore are not rigidly fixed in these compounds, the molecular mechanics program AMBER[28] was employed to search for the conformations of IA, IIA and IIIA most likely to exist in solution. The strategy for this search is described in Experimental.

IA and IIIA were each found to have three unique minimal energy conformations (Table 4). However, the average energy of the low energy conformations of IIIA was 5.6 kcal/mol lower than that of IA. The higher overall energy of IA can be attributed to a sterically-induced distortion of the naphthalene ring and subsequent effects on the dihedral angles within the ring and between the ring and the carboxylate group. This distortion was a result of unfavorable steric interactions between the carbonyl oxygen of the carboxyl group and the hydrogen at position 8 on the naphthalene ring. A rotation of the naphthalene ring by 180° relative to the carboxylate group resulted in greater steric interactions and a more distorted structure. Neither of the other compounds studied displayed this distortion.

In contrast to IA and IIIA, IIA exhibited 8 low energy conformations (Table 4). A single conformer exhibited both the lowest energy and shortest ring to nitrogen distance. Seven other conformers had an average energy that was only 0.7 kcal/mol higher. Because these conformers constituted a large set of thermally accessible states, we were forced to include them in the calculation of average distances. The energies and center-to-center distances of the energetically significant conformations of IA, IIA, and IIIA are summarized in Table 4. Coordinates for each of these conformations are provided in the supplementary material.

The fact that the short-lived fluorescence component of each of these three compounds could be well fit as a single exponential decay suggests either that these conformers interconvert rapidly on the time scale of the quenching (ns to sub-ns), or that conformations populated during the lifetime of the singlet do not differ significantly in their ability to quench the singlet state.

The Förster orientation factor, κ^2, was calculated for the conformers of IA-IIIA (Table 4) as a fairly simple means to compare the relative orientations of naphthalene and nitroxide groups. The absence of large variations in κ^2 suggests that differences in the relative orientation of the two groups is probably not the primary factor controlling the variations in quenching rates among these compounds.

The rates of energy transfer (Förster or Dexter) and electron transfer have well-defined distance dependencies. While the rate of Förster energy transfer follows an R^{-6} distance dependence,[16,29] the rates of Dexter transfer and electron transfer are expected to decline exponentially with distance.[15,17,30,31] However, for aprotic solvents, the observed quenching rates bear no simple relationship to the nitroxide-naphthalene distances (Tables 3 and 4), as is illustrated by the following points: 1) while a comparison between IA and ID suggests that increasing R by 4 Å causes k_q to decrease by about two orders of magnitude, simply shifting the site of substitution from the α (IA) to the β (IIIA) position on the naphthalene ring produces an ~20-fold decrease in k_q, although the values of R for IA and IIIA differ by only 0.76 Å; 2) insertion of a methylene group into the linkage at the α position (IIA) decreases k_q by ~40-fold, although the greater flexibility of this linkage allows a shorter R than either IA or IIIA. As we show below, the rather large variations in k_q observed for compounds having similar nitroxide-naphthalene distances (e.g. IA-IVA) cannot be explained by the differences in the singlet energy of the naphthalenes or by variations in the free energy for photo-induced electron transfer. Instead these variations appear to result from a relationship between k_q and the non-radiative rate constant of the parent (diamagnetic) compound. The presentation and interpretation of this relationship is provided in section D 3.

D. Mechanisms of Quenching

Several mechanisms could contribute to singlet state quenching in these nitroxide adducts. We address here the possible contributions of Förster (dipole-dipole) and Dexter (electron exchange) energy transfer, electron transfer, and electron exchange-induced relaxation to the quenching. In principle, k_q reflects the sum of rate constants for each of these potential relaxation pathways:

(5) $$k_q = k_{FT} + k_{DT} + k_{ET} + k_{EX}$$

1. Energy Transfer

In the light of conflicting reports[1a,1b,1f,12d] as to the importance of Förster and Dexter transfer in the quenching of singlet states by nitroxides, we have re-examined this question. Since no emission is observed from the first excited state of the nitroxide, direct spectroscopic evidence for energy transfer was not obtainable. Instead, we compared the observed quenching rates of IA, IIA, and IIIA to the Förster (J_F) and Dexter (J_D) overlap integrals calculated from the fluorescence spectra of IB, IIB and IIIB, and the absorbance spectrum of 4-hydroxy-2,2,6,6-tetramethyl-1-piperdinyloxy (TEMPOL):

(6a) $$J_F = \frac{\int_0^\infty F(\lambda)\varepsilon(\lambda)\lambda^4 d\lambda}{\int_0^\infty F(\lambda) d\lambda}$$

(6b) $$J_D = \frac{\int_0^\infty F(\lambda)\varepsilon(\lambda) d\lambda}{\int_0^\infty F(\lambda) d\lambda \int_0^\infty \varepsilon(\lambda) d\lambda}$$

where $F(\lambda)$ is the corrected fluorescence intensity of the fluorophore and $\varepsilon_a(\lambda)$ is the extinction coefficient of the acceptor (TEMPOL) at wavelength λ.

The weak nitroxide absorption band overlaps with the red edge of the singlet emission of the naphthyl group. This absorption is solvent dependent[23] (Fig. 4), shifting to the blue

with increasing solvent polarity and thus increasing the values of J_F and J_D. The degree of spectral overlap is further enhanced in polar solvents for compounds IA and IIIA whose emissions shift to the red with increasing solvent polarity (Table 1).

We have used these solvent-dependent changes in the overlap integrals to assess whether the quenching rates vary in the manner expected for energy transfer. The rate constant for Förster transfer is given by, [29]

$$k_{FT} = \frac{J_F \kappa^2 \phi_d}{R^6 n^4 \tau_d} 8.71 \times 10^{23} \qquad (7a)$$

where κ^2 is the orientation factor (Table 4), ϕ_d and τ_p are the quantum yield and lifetime, respectively, of the appropriate diamagnetic O-acetyl derivative (Table 3), R is the donor-acceptor distance (Table 4) and η is the solvent refractive index.

The rate constant for Dexter transfer is given by, [15b]

$$k_{DT} = \frac{4\pi H^2 J_D}{h} = \frac{4\pi^2 H_0^2 e^{-2R/L} J_D}{h} \qquad (7b)$$

where H is the coupling matrix element, H_O is the pre-exponential factor and L is the Bohr radius.

Both of these theories predict that for constant donor-acceptor distance(s) (and orientation(s)) the rate constants for transfer will increase linearly with increasing values of the spectral overlap integrals. However, log plots of k_q vs J_F and J_D for IA, IIA, and IIIA (Fig. 5) clearly do not show this relationship (with the possible exception of IIIA in the Förster plot (Fig. 5)). Furthermore, equation 7a can be employed to calculate k_{FT} from R and κ^2 values (Table 4); these predicted Förster transfer rates (Table 5) are more than an order of magnitude lower than the measured values of k_q. Moreover, choosing a value of 2/3 for κ^2, corresponding to randomized donor-acceptor orientations, [29] increases k_{FT} to a maximum of only ~15% of the observed k_q values. Even in the case of anthracene, where the spectral

overlap with TEMPOL is maximal for the family of linear aromatic ring systems, we calculate that the quenching radius for Förster energy transfer extends to only 9 Å (in ethanol).

We conclude that energy transfer through either a Förster or Dexter mechanism cannot account for the observed magnitude and (lack of) variation in the intramolecular quenching rate constants.

2. Electron Transfer

For electron transfer to be operative, the energy of the excited singlet must be sufficient to drive the relevant redox couple.[30,31] In the absence of Coulombic interactions, the thermodynamic driving force, ΔG_{∞}, is given by[30]

(8) $$\Delta G_{\infty} = -E_{00} + E_{ox} - E_{red}$$

where E_{00} is the 00-excitation energy of the fluorophore, and E_{ox} and E_{red} are the oxidation potential of the electron donor and the reduction potential of the acceptor, respectively.

Assuming a simple continuum model for solute-solvent interaction, additional terms for the Coulombic attraction between the separated charges, ΔG_{Coul}, and for the free energy of solvation of the ion pair, ΔG_{solv} must be included. The total change in free energy is then given by:[30,31]

(9) $$\Delta G_{ET} = \Delta G_{\infty} + \Delta G_{Coul} + \Delta G_{solv}$$

(10a) $$\Delta G_{Coul} = -e^2/\varepsilon R$$

(10b) $$\Delta G_{solv} = \frac{-e^2}{2}\left(\frac{1}{r_d} + \frac{1}{r_a}\right)\left(\frac{1}{\varepsilon_{MeCN}} - \frac{1}{\varepsilon}\right)$$

and e is the electron charge, ε is the solvent dielectric constant, ε_{MeCN} is the dielectric constant of acetonitrile in which the redox potentials were measured, R is the distance between donor and acceptor (Table 4), r_d and r_a are donor and acceptor radii espectively. Coulombic and solvation

adjustments to ΔG_{∞} are greatest (up to +0.8 eV) in hexane ($\varepsilon = 1.88$) and increase steeply with distance in this solvent. For the polar solvents acetonitrile and water, $\Delta G_{Coul} + \Delta G_{solv} <$ 0.1 eV and exhibits little distance dependence.

For IA-IVA, the naphthalene moiety may act as either an electron acceptor or donor resulting in oxidation or reduction, respectively, of the nitroxide; these reactions are shown diagramatically in eqns. 11 and 12:

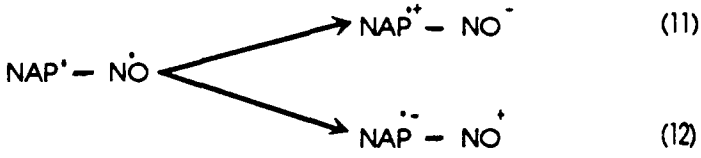

(11)

(12)

acetonitrile both reduction and oxidation of the nitroxide are thermodynamically feasible but that the oxidative pathway (rxn 12) is preferred in all cases by >0.15 eV. In hexane, the lack of solvent stabilization makes reduction of the nitroxide (rxn 11) energetically unfavorable and reduces the driving force for the oxidative pathway ($\Delta G_{ET} > -0.4$ eV). In aqueous solution, nitroxide reduction (rxn 11) has the greater driving force. Although these calculations suggest that the direction of electron transfer would reverse in water, the quenching rate constants do not differ greatly. If electron transfer is the dominant pathway for quenching, transfer in both directions must be occurring with equal facility.

Within individual series of compounds our measured values of k_q do not show any obvious correlation with ΔG_{ET}. For example, the values of k_q for IIA are equal in acetonitrile and hexane, although electron transfer is calculated to be exergonic in the first solvent and endergonic in the latter. Other discrepancies are also apparent. In particular, the k_q's for IIIA and IVA do not vary significantly between acetonitrile and hexane despite the large (~0.8 eV) differences in ΔG_{ET} in these two solvents. Additionally, in polar solvents quenching of IIIA, (β-substituted) is slower than IA (α-substituted) by an order of magnitude although its driving force is greater.

Overall, these data are inconsistent with the notion that electron transfer acts as the dominant pathway for singlet quenching[15a,30,31]. The lack of solvent dependence does not, by itself, rule out electron transfer since the rate of transfer is a function of the activation energy, $\Delta G^{\ddagger}$, which includes an additional solvent dependence in the form of the solvent reorganization energy, λ_S.[30,31] Oevering et al.[30a] have demonstrated that the effect of solvent reorganization on $\Delta G^{\ddagger}$ may in some cases largely compensate for the solvent dependence included in ΔG_{ET}. We were unable to calculate $\Delta G^{\ddagger}$ precisely for these compounds owing to uncertainties in sensitive parameters such as the internal (nuclear) reorganization energy and the effective radius of the nitroxide group. Nevertheless, no reasonable values for these parameters lead to a prediction of faster rates in hexane than in acetonitrile as we have observed for several compounds (IA,D). Based on these observations, we tentatively conclude that electron transfer does not play a major role in the quenching. The complete lack of radical ion formation during singlet state quenching by nitroxides in polar solvents [1f,g] provides additional support for this view. However, owing to the uncertainties in the simple continuum model and the redox potentials for the nitroxides,[2,32,34] as yet, we are hesitant to exclude unequivocally a contribution of electron transfer to the quenching.

3. Electron Exchange

Electron exchange between the naphthoate singlet and nitroxide doublet can produce rapid relaxation of the excited state.[1,14] Available relaxation routes are as follows:[1] (Dexter) energy transfer (13a), intersystem crossing to triplet (13b), or internal conversion (13c)

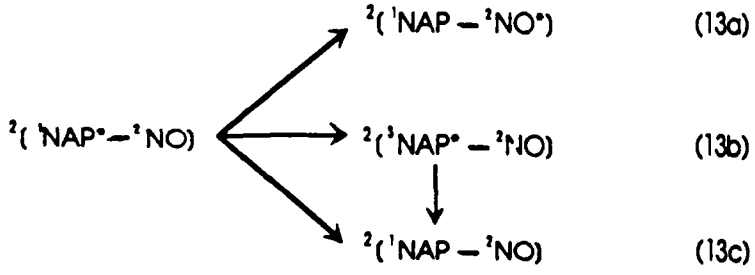

As discussed above Dexter energy transfer is an unlikely relaxation pathway. However, to eliminate energy transfer from consideration and focus on exchange-induced intersystem crossing (13b) or internal conversion (13c), preliminary data were collected on several hematoporphyin-nitroxide adducts (Fig. 6). For these compounds, the energy of the porphyin singlet (~2.0 eV) is well below that of the pyrrolidinyl nitroxide doublet (~2.9 eV) thus eliminating the possibility of Dexter (or Förster) energy transfer. ΔG_{ET} for these adducts is also calculated to be small (- 0.18 eV, nitroxide oxidation)[36]. Nevertheless, in methanol, the rate constants for quenching in the A isomer, 6.6×10^8 s^{-1}, and the B isomer, 7.2×10^8 s^{-1}, are comparable to those of IIA. These results suggest that an electron-exchange induced intersystem crossing to the triplet or internal conversion to the ground state is occurring.

Further support for an exchange induced "local" relaxation is provided by the correlation presented in Fig. 7. Here we have plotted the k_q's of the paramagnetic compounds against the non-radiative rate constants of their corresponding diamagnetic O-acetyl and methyl-ester derivatives. With the exception of IVA in methanol, compounds having similar nitroxide-fluorophore distances (e.g. IA, IIA-IVD) exhibit an approximately linear relationship between these parameters. This correlation is interpreted to result from a fixed enhancement (~55 - fold) by the nitroxide of a pre-existing, non-radiative relaxation pathway in the fluorophore. Because non-radiative decay in most aromatic hydrocarbons proceeds almost exclusively through intersystem crossing (Ermolev's rule[14c]), this enhancement probably reflects a lifting of the spin-restriction to singlet-triplet transition brought about through the coupling of the doublet and excited singlet states.[14] We suspect that the relatively minor deviations from this correlation result from variations in the degree of coupling among these derivatives due to small differences in distance, orientation, and structure (Fig. 1, 6).

If intersystem crossing (13b) competes effectively with triplet quenching by the nitroxide (13b $\rightarrow$ 13c),[3-10] one might expect to see an enhanced phosphorescence signal in nitroxide-substituted compounds as compared with their diamagnetic forms. Observations do not bear this out (Fig. 8); triplet (480 nm) and singlet emission bands are both clearly visible for IA, IB, and ID at 77 K (EPA glass), but for the nitroxide adducts (IA, ID) the triplet emission

is diminished to a greater extent than that of the singlet. Thus we cannot distinguish between pathway 13c and a rapid, two-step relaxation via 13b.

Conclusions

For all adducts examined in this study, absorption and fluorescence emission spectral shapes and energies were identical to those of the parent fluorophore. There was no evidence for charge-transfer absorption or charge-recombination emission. We conclude that the emission arises from the same locally-excited singlet state in the presence or absence of nitroxide substituents.

Intramolecular quenching of excited singlet states by nitroxyl radicals is very efficient; rate constants are in the range of 10^8-10^{10} s^{-1}. At distances as great as 12 Å, the quenching can occurs at rates > 10^8 s^{-1}. The position of ring substitution and the type of linkage appears to significantly influence the quenching efficiency.

Förster energy transfer cannot account for more than a small fraction of the observed rates, even assuming larger values for κ^2. The rates do not show the dependence on overlap integrals predicted by theories of Förster or Dexter energy transfer. There is no clear correlation of k_q values with calculated values of ΔG_{ET}, suggesting that photo-induced electron transfer is also unimportant. Significant quenching rates are obtained in hematoporphyrin-nitroxide adducts which contain a fluorophore whose singlet energy is below that of the lowest excited state of the nitroxide. Since the driving force for electron transfer is also small, this result suggests that the nitroxide moiety facilitates either intersystem crossing to the triplet or internal conversion to the ground state. Further support for exchange-induced relaxation is provided by the linear correlation between k_{nr} and k_q, indicating a fixed enhancement of a pre-existing pathway. Thus we conclude that the quenching arises primarily through electron exchange. This conclusion is consistant with earlier studies of diffusional quenching of aromatic hydrocarbons by nitroxides.[1b]

This work provides the first preliminary evidence for long-range quenching by electron exchange that proceeds via the local relaxation of the singlet and not energy transfer. That this

pathway also appears to outcompete or to occur in preference to exergonic electron transfer is somewhat surprising, given current thinking on the relationship between electron exchange and electron transfer processes.[15b,30b,42] While compounds containing fluorophores with different structures, singlet energies, and redox potentials could, in principle, exhibit a number of different quenching mechanisms, data from this and previous studies[1] have failed to provide unequivocal evidence for the operation of mechanisms other than electron exchange in the quenching of excited singlet states by nitroxides. Further work employing a series of differing nitroxides and fluorophores combined within a rigid structural framework[15] could provide additional insight concerning the factors controlling the possible relaxation pathways.

Experimental

Optical Measurements

Solutions for optical measurements in all solvents were prepared from concentrated (~10 mM) stock solutions in methanol. All solvents were HPLC grade (Aldrich) used without further purification. Absorption spectra were measured on solutions in 1 or 5 cm quartz cells using a Hewlett-Packard 8451A diode array spectrophotometer (spectral resolution, 2 nm).

Quantum yield measurements were made on an SLM-Aminco SPF-500C spectrofluorometer linked to an IBM-XT for data collection and processing. Freshly made solutions had optical densities of $\leq$0.02 at the excitation wavelength, chosen as the absorbance maximum in the range of 280-300 nm. Excitation and emission bandpasses were 2 nm in most cases; 4 nm bandpasses were used to measure some of the very low quantum yields. Samples were thermostated at 20°C. Solutions were deoxygenated through bubbling with N_2; emission scans were repeated until bubbling caused no further increase in fluorescence intensity. Any signal due to the solvent was removed by subtraction. Spectra were corrected for instrumental response and integrated using correction factors and software provided by the manufacturer. (A modified correction procedure was used to avoid arbitrary normalization and conversion steps in the standard routines).

Quantum yields were calculated with respect to quinine sulfate in 0.1 N H_2SO_4 (OD = 0.02) and corrected for refractive index differences between solvents, using

$$\phi = \frac{F_s A_{qs} n_s^2 \phi_{qs}}{A_s F_{qs} n_0^2} \quad (14)$$

where the subscript s refers to the sample, qs refers to quinine sulfate, ϕ is quantum yield, A is absorbance at the excitation wavelength, F is the integrated, corrected fluorescence, n_S is the refractive index of the sample solvent, and n_O is the refractive index of water. ϕ_{qs} is 0.55.

Fluorescence lifetimes were measured by time correlated single photon counting, on an instrument generously made available through the Laser Biomedical Research Center at MIT. Excitation was provided by a cavity-dumped tunable dye laser, synchronously pumped with the second harmonic of a mode-locked Nd-YAG (Coherent, Antares 76-S). For the naphthalene derivatives the dye pulses (5 ps fwhm, 20 MHz) were frequency doubled with a phase matched KTP crystal to 295 nm. The porphyrin derivatives were excited directly with the dye laser, tuned to 580 nm. Fluorescence from deoxygenated samples was collected at 90° (naphthalene derivatives) or 180° (porphyrin derivatives) and focused into a Spex monochometer; entrance and exit slits were adjusted to obtain a counting rate of 4000-5000 photons per second impinging on the PMT.

A Canberra 2143 time-amplitude converter (TAC) received start pulses directly from the cavity dumper and stop pulses from the PMT. The TAC signal is passed to a multi-channel analyzer and the data are saved in an IBM-XT for later analysis with a Sun microcomputer. The instrumental response limit for this system is about 70 ps.

Determination of minimal-energy conformations of IA-IIIA

The general strategy for this search was to allow the functional groups of each compound to freely rotate around all nonconjugated bonds that were not in constrained ring structures. There were two degrees of rotational freedom in IA and IIIA: 1) the bond between the carboxyl carbon and oxygen atoms of the ester linkage; and 2) the carboxyl oxygen and carbon C1 of the nitroxyl ring. The functional groups were rotated through 360° around each

of these two bonds in 5° increments. The structures after each rotation were energy minimized using AMBER[28] to optimize the bond distances, bond angles, dihedral angles of the bonds, dipole and van der Waal's interactions. The structures were allowed to minimize to a convergence of 1.0×10^{-1} kcal/mol difference in overall energy, and 0.10 kcal/mole Å in the gradient of the overall energy. An analysis of the energies associated with each rotation versus the angle of rotation around each degree of freedom showed that the local energy wells were greater than +/-10° in width relative to the angles of the minimized conformations. Thus a smaller rotational increment was not necessary in searching for the global energy minima.

The addition of a methylene group between the naphthalene ring and the carboxylate introduces two additional degrees of rotational freedom to IIA. To simplify this system, the structure was allowed to energy minimize in terms of only the naphthalene ring and the intervening methylene group. This fixes the methylene hydrogens in orientations that are not sterically hindered by the aromatic ring. The structure was then treated in the same fashion as IA and IIIA through rotations around the two carbon-oxygen bonds in the ester linkage, but also including the additional rotation about the methylene-carboxylate bond.

Preparation of Nitroxide Derivatives

General

All starting materials and reagents were obtained from Aldrich and used as received. High purity grade Burdick and Jackson solvents were used following distillation over CaH_2 in all preparations. Chromatographic separation was obtained on a flash column using 30 micron silica (Amicon or Davisil) under positive N_2 pressure, solvents are indicated where appropriate. Melting points, which are uncorrected, were measured on a Mel-temp apparatus (Laboratory Devices). Infrared (IR) spectra were recorded as a thin film on a Mattson Sirrus 100 infrared spectrometer at 4 cm^{-1}. Mass spectra (MS) were obtained by thermal desorption from a copper probe, in either an electron impact (EI) or chemical ionization (CI) mode on a Finnigan 4510 spectrometer interfaced with an INCOS 2300 data system. CI mass spectra of nitroxide derivatives gave an $(M + 2)^+$ molecular ion suggesting the nitroxide derivative is chemically

reduced prior to ionization in the mass spectrometer. This was not observed in the spectra of nitroxides obtained by EI or in the spectra of the nitroxide-acetyl derivatives by CI. Nuclear Magnetic Resonance (NMR) spectra of the acetyl derivatives were obtained on either a Bruker AM-250 or Varian XL-300 at Massachusetts Institute of Technology and measured in $CDCl_3$.

4-(2,2,6,6-tetramethylpiperidinyloxy, free radical) 1-naphthoate (1A). 1-Naphthoyl chloride (950 mg) was dissolved in methylene chloride (10 ml) and pyridine (1 ml). 4-Hydroxyl-TEMPO (860 mg in 2.0 ml of methylene chloride) was added drop wise to the stirred solution. After 20 h this solution was diluted with methylene chloride, washed with water, dried (Na_2SO_4) and evaporated to an orange oil which later crystallized on standing. Column chromatography (BIO-RAD, BIO-SIL A 100-200 mesh) eluting with methylene chloride and recrystallization from methanol afforded the desired product as orange needles: 962 mg; mp 100-102° C; IR 1713 cm^{-1}; MS(EI) 326 (M^+, 18), 155 (100), MS(CI) 328($[M + 2H]^+$, 25), 312 (M - 14,35), 310(M - 16,45), 156 (100).

2-[4-(2,2,6,6-tetramethylpiperidinyloxy, free radical)] 6-hydrogen naphthylenedicarboxylate (IVA) and 2,6-Di[4-(2,2,6,6-tetramethylpiperidinyloxy, free radical)] naphthylenedicarboxylate (IVC). 2,6-Naphthalenedicarboxylic acid (3.5 g) was suspended in methylene chloride (100 ml) and pyridine (3.0 ml). Thionyl chloride (3.0 ml) was then added dropwise and the resultant solution was stirred until no suspension remained and the solution was clear. The intermediate diacid chloride was evaporated to dryness in an effort to remove extraneous thionyl chloride then dissolved in methylene chloride (150 ml) and pyridine (3.0 ml). 4-Hydroxy-TEMPO (1 g) in a small amount of methylene chloride was added and this mixture stirred overnight. Water (3.0 ml) was added and the precipitated diacid was filtered off and washed with excess methylene chloride. The combined filtrate was washed with water, dried with anhydrous sodium sulfate and evaporated to a dark orange oil. The desired products were separated and purified by flash chromatography (eluting with 3% methanol/methylene chloride) and recrystallized from methanol giving compound IV A (90 mg) and compound IV D (220 mg). Compound IVA: mp > 200° C(dec); IR 3200-2200 cm^{-1} (b), 1715, 1622 cm^{-1}; MS(EI)

370(M^+), 199(80), 124(100). Compound IVD: mp > 225° C(dec); IR 1712 cm^{-1}; MS(EI) 524(M^+, 30), 370(20), 124(100).

4-(2,2,6,6-tetramethylpiperidinyloxy, free radical) 2-naphthoate (IIIA). 2-Naphthoyl chloride (380 mg) and 4-Hydroxy-TEMPO (345 mg) were dissolved in cold pyridine and stirred overnight (20 hr). This mixture was diluted with methylene chloride, washed with water (1 x 25 ml), 1 HCl (3 x 25 ml), dried over an hydrous sodium sulfate, and evaporated to dryness. The desired product was purified by flash chromatography (methylene chloride), obtained as a solid and recrystallized from methylene chloride/n-hexane: 235 mg; mp 122-123° C; IR 1713 cm^{-1}; MS(CI) 328 $[M + 2]^+$, 75), 312(M - 14,70), 310(M - 16,50), 156(100).

4-(2,2,6,6-tetramethylpiperidinyloxy, free radical) (1-naphthyl) acetate (IIA). 1-Naphthylacetic acid (500 mg) was combined with dicyclohexylcarbodiimide (DCC, 610 mg), dimethylaminopyridine (DMAP, 32 mg) and 4-Hydroxy-TEMPO (462 mg) and dissolved in methylene chloride and stirred overnight under an atmosphere of N_2[37]. The solid dicyclohexyl urea was filtered off and further rinsed with methylene chloride. The combined filtrate was washed with 1N HCl (2 x 75 ml), water (3 x 75 ml), dried (Na_2SO_4) and evaporated. The product was purified by flash chromatography (methylene chloride) and evaporated to an orange oil which did not crystallize: IR 1733 cm^{-1} MS(CI) 342($[M + 2]^+$, 25), 326(M - 14,40), 324(M - 16,38), 156(100).

4-[17β-hydroxy-4,4'-dimethylspiro (5α-androstane-3,2'-oxazolidin)-3'yloxy, free radical] 1-naphthoate(ID). Compound ID was prepared by the DCC coupling described above using 1-Naphthoic acid and 3-DOXYL-17β-hydroxy-5 α-androstane (Aldrich). The desired product was purified by TLC on a 1 mm thick plate (20 x 20 cm, Whatman) eluted with methylene chloride and obtained as a yellowish solid: mp 153 - 154° C; IR 1714 cm^{-1}; MS(EI) 530(M^+, 1), 444(DOXYL fragment loss, 2), 155(100).

Preparation of Nitroxide-Acetyl Derivatives

4-(2,2,6,6-tetramethylpiperidinylacetoxy) 1-naththoate (IB). Compound IA (50 mg) dissolved in tetrahydrofuran (3 ml) in the presence of 5% palladium/carbon (5 mg) was

stirred under an atmosphere of hydrogen for 3 h. After this time the solution was filtered directly (with minimal exposure to air) into a solution of acetic anhydride/pyridine (1:10) which had been previously deoxygenated with nitrogen. This solution was stirred for 20 h under N_2 then diluted with methylene chloride, washed with water, dried, and evaporated to a yellowish oil. After chromatography on silica (eluting with methylene chloride) fractions containing product crystallized after solvents were removed. The final product was recrystallized from methanol to remove a small amount of compound IA and gave a snowy white solid: 20 mg; mp 86-87° C; IR 1712, 1770 cm^{-1}; MS(EI) 369(M^+), 327(M^+ - 42), 155(90), 140(100); NMR(250 MHz) δ 8.80(d), 8.14(d), 8.02(d), 7.88(d) 7.55(m) (7H,2,3,4,5,6,7,8 -H), 5.45 (m, 11 -H), 2.13(s,OCOMe), 2.20 - 2.00(m, 4H, 12 -CH_2), 1.35, 1.17(s, 12H, 13a -Me).

2-[4-(2,2,6,6-tetramethylpiperidinylacetoxy)] 6-hydrogen naphthylenedicarboxylate (IVB). 2,6-Di[4-(2,2,6,6-tetramethylpiperidinylacetoxy)] naphthylenedicarboxylate (IVE), 4-(2,2,6,6-tetramethylpiperidinylacetoxy) 2-naphthoate (IIIB), 4-(2,2,6,6-tetramethylpiperidinylacetoxy) (1-naphthyl)acetate (IIB). These compounds were prepared in a fashion analogous to compound IB. However, the hydroxylamine produced in the catalytic reduction of compound IVA precipitated upon its formation and excess tetrahydrofuran and pyridine was added in order to filter off the catalyst. Compound IVB was not purified chromatographically but was obtained as a white solid from crystallization in methanol. Compound IVB: IR 1769, 1753, 1715 cm^{-1}; MS(EI) 413(M^+), 371 (M^+ - 42), 140(100); NMR(250 MHz) δ 8.74, 8.61 (s,1,5 -H), 8.22(d), 8.18(m)(4H 3,4,7,8 -H), 5.45(m, 12 -H), 2.16(s, OCOMe), 2.11(m, 4H, 13 -CH_2), 1.34, 1.18(s, 12H, 14 -Me).

Compound IVE: IR 1766, 1703 cm^{-1}; MS(EI) 610(M^+,5), 568(M^+ -42,30), 124(100); NMR(250 MHz) δ 8.58(s, 1,5 -H), 8.04(m,3,4,7,8 -H), 5.43(m,12 -H), 2.13(s, OCOMe), 2.03(m,4H, 13 -CH_2), 1.33, 1.16(s, 12H, 14 -Me).

Compound IIIB: mp 115-116° C IR 1732 cm^{-1}, MS(CI) 398 (M + 29,5), 370([M + 1]$^+$, 100), 310(M - CH_3CO_2H,95), 198(30), NMR(250 MHz) δ 8.54(s, 1H, 1-H), 8.00(d),

7.94(d), 7.86(d), 7.55(m) (6H, 3,4,5,6,7,8 -H), 5.39(m, 11 -H), 2.11(s,OCOMe), 2.15 - 1.90 (m, 4H, 12 -CH_2), 1.31, 1.14(s, 12H, 13a-Me).

Compound IIB: IR 1767, 1732 cm^{-1}, MS(CI) 412(M + 29,5), 384($[M + 1]^+$, 100), 324 (M - CH_3CO_2H, 100), 198(45), NMR(250 MHz) δ 7.96(d), 7.84(d), 7.77(d), 7.49(m), 7.38(m)(7H, 2, 3, 4, 5, 6, 7, 8 -H), 5.06 (m, 11 -H), 4.02(s, 2H, 1a-CH_2), 2.06(s, OCOMe), 1.90 - 1.67(m, 4H, 12 -CH_2), 1.17, 1.04(s, 12H, 13a-Me).

Preparation of Methyl Esters

Methyl 1-naphthoate (IC) and Methyl 2-naphthoate (IIIC). 1-Naphthoyl chloride (500 mg) 1 or 2-Naphthoyl chloride was dissolved in cold pyridine (3 ml), methanol (2 ml) was added, and the resultant mixture was stirred in an ice bath for 2 hr and at room temperature for an additional 4 hr after which the reaction mixture was diluted with methylene chloride, washed with water (1 x 25 ml), 1M HCl (3 x 25 ml), water (2 x 25 ml) , dried (Na_2SO_4), and evaporated to dryness. The product was purified by flash chromatography (methylene chloride). Compound IC: obtained as a colorless oil; IR 1711 cm^{-1}. Compound IIIC: obtained as a solid and recrystallized from methylene chloride/n-hexane mp 72 - 73° C, IR 1711 cm^{-1}, MS(CI)215($[M + 29]^+$, 15), 187($[M + 1]^+$, 100), 155(10).

2-Methyl 6-hydrogen naphthylenedicarboxylate (IVC), 2,6-dimethyl naphthodylenedicarboxylate (IVF) and Methyl 1-(naphthyl)acetate (IIC). Compounds IVC and F were prepared by the procedure used in the synthesis of compounds IVA and D substituting methanol for 4-Hydroxy-TEMPO. Compound IVC: mp > 200° C (dec.), IR 1721, 1682 cm^{-1}, MS(CI)259(M + 29,15), 231($[M + 1]^+$, 100),NMR (250 MHz, $CDCL_3$ and d_5-pyridine) δ 8.69, 8.61(s,1,4 -H), 8.20(d of d), 8.08(d of d), 7.98(d) (4H, 3, 4, 7, 8 -H), 3.96 (s, 3H, 2a-OMe). Compound IVE: mp 188° C (lit. 186° C), IR 1707 cm^{-1}. Compound IIC was prepared by the procedure used for the synthesis of compound IIB substituting methanol for the nitroxide: obtained as a colorless oil; IR 1736 cm^{-1}; MS(CI) 229($[M + 29]^+$, 8), 201($[M + 1]^+$, 100), 169($[M + 1]^+$ -OMe, 65).

Preparation of Hematoporphyrin IX carboxy-PROXYL Derivatives

2(4)-Vinylhematoporphyrin IX DME was obtained from commercial hematoporphyrin IX (Aldrich) by the H_2SO_4/methanol procedure reported by Smith.[38] The product was purified by flash column on silica (3 - 5% methanol/methylene chloride) and obtained as a solid from methylene chloride/n-hexane. At this point, no effort was made to resolve the isomeric mixture of 2(4)-Vinylhematoporphyrin IX DME.

Vinylhematoporphyrin IX DME IR 3442 cm^{-1}(bd, O - H), 3319 (m, N-H), 1734(s, ester C=O); MS(CI)637($[M + 29]^+$, 8), 609($[M + 1]^+$, 70),591($[M + 1]^+ - H_2O$, 100); NMR (300 MHz) δ 10.18, 10.06, 10.01, 9.93, 9.91, 9.88 (4H,a,b,g and d meso -H), 8.20 (m, 1H, 2a and 4a -H of vinyl), 6.35, 6.17 (m, 3H, 2a and 4a -H of hydroxyl ethyl and 2b and 4b $-CH_2$), 4.31 (4H, 6a and 7a-CH_2), 3.65, 3.61, 3.55, 3.53, 3.50, 3.43, 3.42 (overlapping s's, 18H, 1,3,5,8 -Me and 6,7 -OMe), 3.23 (t, 4H, 6b and 7b -CH_2), 2.12 (d, 3H, 2a and 4a-Me).

2(4)-1[-(hydroxy)ethyl]-4(2)-ethyl-6,7-bis[2-(methoxycarbonyl)ethyl]-1,3,5,8-tetramethylporphyrin (VC)

2(4)-Vinylhematoporphyrin IX DME dissolved in tetrahydrofuran in the presence of 5% palladium/carbon (5 mg) was stirred under an atmosphere of hydrogen overnight. After filtering off the catalyst the desired product was purified on a flash column (3% methanol/methylene chloride) and obtained as a solid: IR 3454 cm^{-1} (bd, O - H), 3318 (m, N - H), 1735 (s, ester C=O); MS(CI) 639 ($[M + 29]^+$, 10), 611($[M + 1]^+$, 100), 593($[M + 1]^+ - H_2O$, 95); NMR(300 MHz) δ 10.34, 10.03, 10.01, 10.00, 9.99, 9.97(4H,a,b,g and d meso -H), 6.32(q, 1H, 2a and 4a -H of hydroxy ethyl), 4.34 (m, 4H, 6a and 7a-CH_2), 4.05 (m,2H,2a and 4a -CH_2), 3.66, 3.65, 3.64, 3.57, 3.56, 3.55 (overlapping s's, 18H, 1,3,5,8-Me and 6,7-OMe), 3.25(t,4H,6b and 7b-CH_2), 2.14(d,3H,2a and 4a-Me of hydroxy ethyl), 1.84(t,3H,2a and 4a-Me of ethyl).

2(4)-(1-[3-(2,2,5,5-tetramethylpyrrolidinyloxy, free radical)carbonyloxy])ethyl-4(2)-ethyl-6,7-bis[2-(methoxycarbonyl)ethyl]-1,3,5,8-tetramethylporphyrin (VA,B). The nitroxide derivative was prepared by the DCC coupling reaction with 3-carboxy-PROXYL and the hydroxy porphyrin. A and B isomers

were separated by TLC (3% methanol/methylene chloride) but were not uniquely identified as to substituant position (2 or 4).

2(4)-carboxy-PROXYL-4(2)-ethylhematoporphyrin IX DME (VA): IR 3316 cm^{-1}; (m,N -H), 1735(s,ester c=O); MS(CI)807($[M + 29]^+$, 1), 779($[M + 1]^+$,3), 764($[M + 1]^+$ -15,8), 593($[M + 1]^+ - H_2O$, 100).

Supplementary Material Available: A listing of atomic coordinates for low energy conformations of IA, IIA and IIIA (8 pages). Ordering information is given on any current masthead page.

Acknowledgements

This work was supported by the Office of Naval Research under ONR Contract N00014-87-K-007 and Grant N00014-89-J-1260 (N.V.B.), and ONR Contract N00014-88-K-0388 (P.S.H.). Partial support for SG was provided by the Environmental Protection Agency.

Fluorescence lifetime measurements were made possible through MIT's Laser Biomedical Research Center, an NIH funded facility at the George R. Harrison Spectroscopy Laboratory. We also thank K. An for help with the lasers and data deconvolution. This is contribution No. 7348 from the Woods Hole Oceanographic Institution.

References

(1) (a) Buchachenko, A.L.; Khloplyankina, M.S.; Dobryakov, S.N. Opt. Specktrosk. (USSR) 1967, 22, 554-556.

(b) Green, J.A.; Singer, L.A.; Parks, J.H. J. Chem. Phys. 1973, 58, 2690-2695.

(c) Darmanyan, A.P.; Tatikolov, A.S. J. Photochem. 1986, 32, 157-163.

(d) Watkins, A.R. Chem. Phys. Lett. 1974, 29, 526-528.

(e) Kuzmin, V.A.; Tatikolov, A.S. Chem. Phys. Lett. 1977, 51, 45.

(f) Chattopadhyay, S.K.; Das, P.K.; Hug, G.L. J. Am. Chem. Soc. 1983, 105, 6205-6210.

(g) Yee, W.A.; Kuzmin, V.A.; Kliger, D.S.; Hammond, G.S.; Twarowski, A.J. J. Am. Chem. Soc. 1979, 101, 5104.

(2) Samanta, A.; Bhattacharyya, K.; Das, P.K.; Kamat, P.V.; Weir, D.; Hug, G.L. J. Phys. Chem. 1989, 93, 3651.

(3) (a) Singer, L.A.; Davis, G.A. J. Am. Chem. Soc. 1967, 89, 158.

(b) Singer, L.A.; Davis, G.A.; Muralidharan, V.P. J. Am. Chem. Soc. 1969, 91, 897.

(4) (a) Yang, N.C.; Loeschen, R.; Mitchell, D. J. Am. Chem. Soc. 1967, 91, 5465.

(b) Chapman, O.L.; Koch, T.H.; Klein, F.; Nelson, P.J.; Brown, E.L. J. Am. Chem. Soc. 1968, 90, 1657.

(5) (a) Schwerzel, R.E.; Caldwell, R.A. J. Am. Chem. Soc. 1973, 95, 1382.

(b) Caldwell, R.A.; Schwerzel, R.E. J. Am. Chem. Soc. 1972, 94, 1035-1037.

(6) Gijzeman, O.L.J.; Kaufman, F.; Porter, G. J. Chem. Soc. Faraday Trans. II 1973, 69, 727-737.

(7) Watkins, A.R. Chem. Phys. Lett. 1980, 70, 262.

(8) (a) Kuzmin, V.A.; Tatikolov, A.S.; Borisevich, Yu. E. Chem. Phys. Lett. 1978, 53, 52.

(b) Kuzmin, V.A.; Tatikolov, A.S. Chem. Phys. Lett. 1978, 53, 606.

(c) Borisevich, Yu. E.; Kuzmin, V.A.; Renge, I.V.; Darmanyan, A.P. Izvest. Akad. Nauk. SSSR 1981, 9, 2014.

(d) Borisevich, Yu. E.; Kuzmin, V.A.; Kokorin, A.I.; Sennikov, G.P.; Novozhilova, G.A.; Shapiro, A.B. Izvest. Akad. Nauk. SSSR 1981, 9, 2019.

(9) Kuzmin, V.A.; Kliger, D.S.; Hammond, G.S. Photochem. Photobiol. 1980, 31, 607.

(10) Chattopadhyay, S.K.; Kumar, C.V.; Das, P.K. J. Photochem. 1985, 30, 81.

(11) Green, J.A.; Singer, L.A. J. Am. Chem. Soc. 1974, 96, 2730.

(12) (a) London, E. Mol. Cell. Biochem. 1982, 45, 181 and references contained therein.

(b) Chattopadhyay, A.; London, E. Biochem. 1987, 26, 39.

(c) Winiski, A.P.; Eisenberg, M.; Langner, M.; McLaughlin, S. Biochem. 1988, 27, 386.

(d) Puskin, J.S.; Vistnes, A.I.; Coene, M.T. Arch. Biochem. Biophys. 1981, 206, 164.

(13) (a) Atik, S.S.; Singer, L.A. J. Am. Chem. Soc. 1978, 100, 3234.

(b) Atik, S.S.; Kwan, C.L.; Singer, L.A. J. Am. Chem. Soc. 1979, 101, 5696.

(c) Atik, S.S.; Singer, L.A. Chem. Phys. Lett. 1978, 59, 519.

(d) Scaiano, J.C.; Paraskevopoulos, C.I. Canad. J. Chem. 1984 62, 2351.

(14) (a) Hoytink, G.J. Acc. Chem. Res. 1969, 2, 114.

(b) Birks, J.B. Photophysics of Aromatic Molecules, 1970, Wiley-Interscience, London, pp 492-517.

(c) Turro, N.J. Modern Molecular Photochemistry, 1978, Benjamin-Cummings Pub. Co. Inc., Menlo Park, chap. 6.

(15) (a) Closs, G.L.; Calcaterra, L.T.; Green, N.J.; Penfield, K.W.; Miller, J.R. J. Phys. Chem. 1986, 90, 3673.

(b) Oevering, H.; Verhoeven, J.W.; Paddon-Row, M.N.; Cotsaris, E; Hush, N.S. Chem. Phys. Lett. 1988, 143, 488.

(16) Förster, T. Ann. Phys. (Leipz.) 1948, 2, 55.

(17) Dexter, D.L. J. Chem. Phys. 1953, 21, 836.

(18) Blough, N.V.; Simpson, D.J. J. Am. Chem. Soc. 1988, 110, 1915.

(19) Kieber, D.J.; Blough, N.V., Free Rad. Res. Comm., In Press

(20) Gerlock, J.L.; P.J. Zacmanidis, D.R. Bauer, D.J. Simpson, N.V. Blough, and I.T. Salmeen, Free Rad. Res. Comm. in press.

(21) Blough, N.V. Environ. Sci. Techn. 1988, 22, 77.

(22) (a) Kikuchi, O. Bull. Chem. Soc. Jpn. 1969, 42, 47.

(b) Salotto, A.W.; Burnelle, L. J. Chem. Phys. 1970, 53, 333.

(23) (a) Briere, R.; Lemaire, H.; Rassat, A. Bull. Soc. Chim. Fr. 1965, 3273.

(b) Mukerjee, P.; Ramachandran, C. and Pyter, R.A., J. Phys. Chem. 1982, 86, 3189-3197.

(24) Kosower, E.M.; Huppert, D. Ann. Rev. Phys. Chem. 1986, 37, 127.

(25) Davidson, R.S. Adv. Phys. Org. Chem. 1983, 19, 1a

(26) Blough, N.V. and D.J. Kieber, work in progress.

(27) A long-lived component present at a level of 3% could contribute as many as 50% of the photons to the measured quantum yield. This would result in an underestimate of k_q by a factor of two. Quenching constants reported here, therefore, represent a lower limit for quenching rates in IA.

(28) Weiner, P.K.; Kollmann, P.A., J. Comput. Chem. 1981, 2, 287.

(29) Lakowicz, J.R., Principles of Fluorescence Spectroscopy, 1983, Plenum Press. N.Y., p 305.

(30) (a) Oevering, H.; Paddon-Row, M.N.; Heppener, M.; Oliver, A.M.; Cotsaris, E.; Verhoeven, I.W.; Hush, N.S., J. Amer. Chem. Soc. 1987, 109, 3258.

(b) Kavarnos, G.J.; Turro, N.J., Chem. Rev. 1986, 86, 401-499.

(31) Marcus, R.A; Sutin, N. Biochim. Biophys. Acta. 1985, 8111, 265 and references contained therein.

(32) Fish, I.R.; Swarts, S.G.; Sevilla, M.D.; Malinski, T., J. Phys. Chem. 1988, 92, 3745.

(33) Tsunaga, M.; Iwakura, C.; Tamura, H., Electrochim. Acta 1973, 18, 241.

(34) While the oxidation potential of TEMPOL exhibits only a slight solvent dependence, its reduction is apparently more favorable by as much as 1 eV in protic solvents, perhaps due to stabilization of the reduced species by protonation. (ref. 32).

(35) (a) DeLuca, C.; Giomini, C.; Rampazzo, L., J. Electroanal Chem. 1986, 207, 161

(b) Siegerman, H. in "Technique of Electrorganic Synthesis Part II, Weinberg, N.L. editor, 1975, John Wiley & Sons, Inc., New York

(c)Klopman, G.; Nasielski, I., Bull. Soc. Chim. Belg. 70, 490 (1961)

(36) Driving force calculation is based on porphyrin reduction potential of -1.34 V vs. SCE (ref. 39) and PROXYL oxidation potential of +0.62 V (ref. 32). Driving force for porphyrin oxidation/nitroxide reduction is +0.4 V.

(37) Hassner, A.; Alexanian, V., Tetrahedron Letters, 1978, 46, 4475-4478.

(38) Smith, K.M. (ed.); Porphyrins and Metalloporphyrins, 1975, Elsevier Scientific Publishing Co.

(39) Felton, R.H.; in The Porphyrins, D. Dolphin, ed., 1978, Academic Press.

(40) Suzuki, S.; Fujii, T.; Ishikawa, T., F. Mol. Spectrosc. 1975, 57, 490.

(41) Orchin, M.; Jaffe, H.H., Symmetry, Orbitals and Spectra, 1971, John Wiley and Sons, Inc., New York, pp. 204-230.

(42) Closs, G.L.; Johnson, M.D.; Miller, J.R.; Piotrowiak, P., J. Am. Chem. Soc., 1989, 111, 3751.

(43) Andreoni, A.; Cubeddu, R.; De Silvestri, S; Jori, G.; Laporta, P.; Reddi, E., Z. Naturforsch., 1983, 38, 83.

Figure Captions

Figure 1. Naphthalene derivatives examined in this study.

Figure 2. Fluorescence excitation and emission spectra of IVD in hexane.

Figure 3. Fluorescence decays of nitroxide adducts (b) as compared to diamagnetic analogues (a): (1) ID and IB in acetonitrile, (2) ID and IB in hexane, (3) IIA and IIB in acetonitrile, (4) IIIA and IIIB in acetonitrile. Excitation wavelength was 295 nm. Emission was monitored at the peak maximum for each compound (see Table 1).

Figure 4. Absorption spectra of TEMPOL in a series of solvents showing the solvent-dependent shifts in the absorption maximum and extinction coefficients (M^{-1} cm^{-1}). Fluorescence emission spectrum of IB in methanol is included in order to illustrate the degree of spectral overlap between naphthalene emission and nitroxide absorption.

Figure 5. Intramolecular quenching constants vs spectral overlap integrals for IA(■), IIA(▲), and IIIA(●); (a) Förster spectral overlap integral, J_F ($M^{-1}cm^3$). The rate constants have been normalized, $k'=k_q \tau_d n^4/\phi_d$, to account for solvent dependent variations in lifetime, quantum yield and refractive index. (b) Dexter spectral overlap J_D (cm).

Figure 6. Hematoporphyrin derivatives examined in this study. The two isomers (V A and B) with the nitroxide at either the 2 or 4 position were separated, but were not uniquely identified.

Figure 7. Intramolecular quenching constants (k_q) of nitroxide adducts IA(■), IIA(▲), IIIA(●), IVA(△), IVD(x), and VA(*) vs non-radiative rate constants (k_{nr}) of the corresponding diamagnetic O-acetyl and methyl ester derivatives. k_q values for IVD are divided by two to account for the presence of two nitroxide groups in this compound. The line represents a linear regression (slope = 0.96, $r^2 = 0.76$) of all data excluding IVA in methanol (circled) and VA. k_{nr} for VA in methanol was estimated from data of Andreoni, et.al.[43]

Figure 8. Fluorescence (1) and phosphorescence (2) emission spectra of IA, IB, and ID. Excitation wavelength, 300 nm; bandpass, 2 nm; concentration,15 μM in EPA glass, 77 K. Phosphorescence intensities are expanded by a factor of 5.

Table 1. Absorption and fluorescence maxima of I-IV[1]

	absorbance in methanol		fluorescence emission maxima (nm)			
compounds	abs max (nm)	ε ($M^{-1} cm^{-1}$)	hexane	acetonitrile	methanol	water
Series I	222	4.2×10^4	332	361	369	390
	300	7.1×10^3	343			
			358			
Series II[2]	228	-	328	326	326	325
	274		340	335	337	335
	284		318	353		
	294		352	371		
Series III	242	1.9×10^4 (8.9×10^4)	336	344	364	376
	276	7.9×10^3	352	359	351	
	284	9.6×10^3 (1.3×10^4)	367	375		
	296	6.8×10^3 (9.7×10^3)	388			
	324	1.6×10^3 (2.2×10^3)				
	338	1.9×10^3 (2.7×10^3)				
Series IV A-C	248	7.0×10^4	355	359	359	360
	288	1.2×10^4	373	377	374	381
	298	1.1×10^4	393	397	396	
	334	1.8×10^3	416	426		
	348	2.0×10^3				
IV D-F	246	8.3×10^4 (8.4×10^4)	354	360	363	
	286	1.4×10^4	372	378	380	
	296	1.4×10^4 (1.3×10^4)	391	400		
	338	2.1×10^3 (2.3×10^3)		425		
	352	2.4×10^3 (2.8×10^3)				

[1]Absorption spectra and extinction coefficients measured in methanol. Values in parentheses are extinction coeffients for methyl esters (III C and IV F) for which the coefficient differs slightly from that of the nitroxide derivative. The nitroxide contributions to the absorption of I-IVA and I,IVD are described in the text and in fig. 4.

[2]Series II compounds were isolated as oils; extinction coeficients were not measured.

Table 2. Fluorescence lifetimes and quantum yields of I-IV[1].

	hexane			acetonitrile			methanol[2]			water[3]		
	τ, ns	ϕ		τ, ns	ϕ		τ, ns	ϕ		τ, ns	ϕ	
Series I												
A	(0.021)[4]	0.002		(0.033)[4]	0.004		(0.054)[4]	0.006		0.10	0.013	(0.009)[4]
B	0.73	0.05		1.7	0.22		2.8	0.31		7.1	0.66	
C	1.00	0.06		1.8	0.20		2.9	0.28		7.3	0.57	
D	0.48	0.03		1.1	0.14		1.1	0.12		-	-	
Series II												
A	1.09	0.004	(0.006)	1.1	0.006	(0.004)	0.81	0.013	(0.004)	0.40	0.008	(0.002)
B	37.0	0.22		33.7	0.13		43.1	0.20		28.3	0.17	
C	49.2	0.22			0.16		43.3	0.21			0.17	
Series III												
A	0.52	0.017	(0.019)	0.50	0.016	(0.011)	0.65	0.026	(0.019)	0.46	0.031	(0.012)
B	9.0	0.33		12.4	0.28		11.0	0.32		10.9	0.28	
C	9.8	0.38			0.30		11.0	0.30			0.32	
Series IV												
A	0.29	0.009	(0.008)	0.33	0.013	(0.012)	0.54	0.010	(0.014)	0.70	0.029	(0.016)
B	14.1	0.40		13.2	0.52		1.1	0.028		12.2	0.28	
C	11.5	0.48		13.7			1.2	0.046		12.3		
D	0.21	0.005	(0.006)	0.22	0.006	(0.007)	0.27	0.008	(0.009)	-	-	
E	15.3	0.46		13.8	0.46		13.9	0.45		-	-	
F	16.1	0.54		15.0	0.50		14.1	0.40		-	-	

[1] Values in parentheses were calculated from equation 3.

[2] Values in methanol are ≈30% lower than those previously reported [18] due to correction of undocumented normalization and conversion routines in the SLM-Aminco software.

[3] "Water" measurements for IV A-C were done in pH 8, 50mM phosphate buffer; I D and IV D-F are not water soluble.

[4] Calculated lifetimes only are reported for IA, except in water, because they were below the time resolution of the instrument. Values were calculated from quantum yields of IA and lifetimes of IB using equation 3.

Table 3. Rate constants for intramolecular quenching in the naphthalene-nitroxide adducts[1]

	$k_q \times 10^{-9}\ s^{-1}$			
compound	hexane	acetonitrile	methanol	water
IA	45	30	18	9.7
I D	0.71 ± .3	0.30 ± .1	0.55 ± .1	-
II A	0.89	0.88	1.2	2.5
IIIA	1.8	1.9	1.4 ± .2	2.1
IVA	3.4	3.0	0.94	1.3
IV D	4.7	4.5 ± .5	3.7 ± .4	-

[1] Rate constants were calculated from fluorescence lifetimes (or quantum yields, in the case of compound I A , see table 2) using Eqn. 4. Uncertainties are ±10% except where otherwise noted.

Table 4. Total energies, nitrogen atom-naphthalene ring distances and κ^2 for lowest energy conformations of IA, ID, IIA, and IIIA.

compound	energy[1] kcal/mol	distance[2], R Å	κ^2 [3]
IA	22.25	8.24	0.18
	22.30	8.26	0.11
	22.39	8.25	0.12
average[4]	22.31	8.25	0.14
ID[5]		12.2	
IIA	14.64	6.55	0.01
	15.01	7.81	0.03
	15.02	7.41	0.16
	15.18	7.94	0.07
	15.42	8.32	0.21
	15.47	8.66	2.01
	15.54	8.83	0.01
	15.80	7.59	0.17
average[6]	15.12	7.59	0.26
IIIA	16.67	9.04	0.21
	16.68	8.94	0.18
	16.74	9.04	0.33
average[4]	16.70	9.01	0.24

[1] Energy for each conformation is the sum of contributions for bond lengths and angles, dihedral bond angles, and dipole and van der Waal's interactions.

[2] Distances were measured from the nitrogen atom to the center of the C9-C10 bond of the naphthalene ring.

[3] κ^2 was calculated[29] from the emission (naphthalene) and absorption (nitroxide) dipoles. Emission dipoles for 1- and 2-substituted naphthaldehydes (^1L_b transition) were obtained from reference 40. The absorption dipole for the nitroxide group was taken to be perpendicular to the NO bond and lying in the CNC plane, based on the local C_s symmetry of the nitroxide group and the analogy to the $n \rightarrow \pi^*$ transition in carbonyls.[15b,22,23,41] $0 < \kappa^2 < 4$, allowed range.

[4] Numerical averages of the energies, distances and κ^2 for the conformations of each compound.

[5] Distance for ID was estimated from molecular models using the same relative orientation of the carbonyl group as that calculated for the lowest energy conformation of IA.

[6] Averages for IIA were weighted according to the population in the lowest energy conformation (E=14.64 kcal/mol) compared with the other seven states ($E_{average}$=15.35 kcal/mol). The ratio of population in states 2-8 relative to state 1 is estimated by: $N_{(2-8)}/N_{(1)}=g_{(2-8)}/g_{(1)} \times \exp(-\Delta E/RT) = 7 \exp(-(15.35-14.64)/RT) = 2.11$.

Table 5. Calculated Förster energy transfer rates[1].

	$k_{FT} \times 10^{-9}\ s^{-1}$			
compound	hexane	acetonitrile	methanol	water
IA	0.016	0.081	0.014	0.150
IIA	0.005	0.004	0.008	0.014
IIIA	0.010	0.009	0.024	0.060
IVA	0.010	0.026	0.025	0.025

[1] k_{FT} calculated from equation 7a using the average values of R and κ^2 (Table 4) and ϕ_d, τ_d values from Table 2; J_F values generated from equation 6a.

Table 6 Singlet energies (E_{00})[1] and calculated thermodynamic driving forces (ΔG_{ET}) for electron transfer.[2]

	hexane[3,4]		acetonitrile[2]		water[5]	
compound	E_{00}	ΔG_{ET}	E_{00}	ΔG_{ET}	E_{00}	ΔG_{ET}
IA	3.82	-0.25	3.43	-0.90	3.18	-1.03
ID[6]	3.82	+0.03	3.43	-0.90		
IIA	4.00	+0.07	4.00	-0.87	4.00	-1.85
IIIA	3.72	-0.07	3.65	-1.12	3.30	-1.14
IVA	3.54	-0.29	3.51	-1.33	3.44	-1.28
IVD	3.54	-0.29	3.52	-1.34	-	-

[1] Singlet energies (E_{00}) were obtained experimentally from the intersection points of fluorescence excitation and emission spectra.

[2] Calculated from equation 8 in text; units are eV.

[3] Favored charge-separated product is (Nap^{-}-NO^{+}). Oxidation potential of TEMPOL (+0.63 V vs. SCE) in acetonitrile from reference 2; reduction potentials for 1-[35], 2-[35b,c] and 2,6-[35a] substituted naphthoates (-1.92 V, -1.95 V, and -1.55 V, respectively), and 1-methyl-naphthalene[35b] (-2.5 V) in dimethylformamide, acetonitrile or 75% dioxane/water were employed to calculate ΔG_{∞} for IA, IIIA, IVA, and IIA respectively.

[4] Values in hexane adjusted for solvation (see text) using eqn 10 and the approximation $r_d=r_a=3.8$ Å.

[5] In water the favored charge-separated product is (Nap^{+}-NO^{-}). The reduction of TEMPO gives an irreversible wave in cyclic voltametry (-0.62 V).[32,33] The oxidation potentials of 1-[35b] and 2-[35b] methyl-naphthalenes (+1.53 V and +1.55 V, respectively) in acetic acid solution were used as the best available estimates for potentials of compounds substituted at the 1 and 2 positions.

[6] Redox potentials for DOXYL were unavailable; the values for TEMPOL were assumed.

Fig. 1, Green, et al

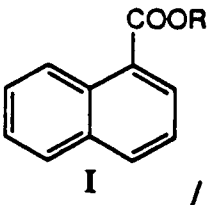

I

I A R = 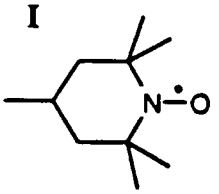

B R = 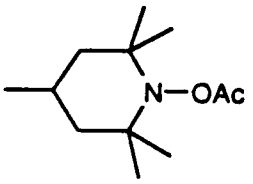

C R = Me

D R = 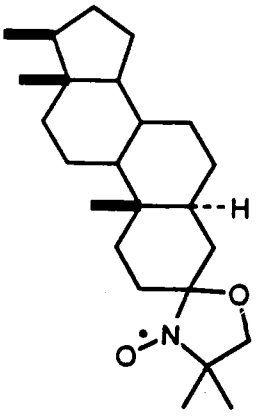

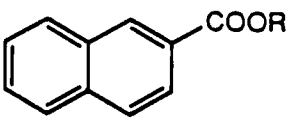

III

III A R = 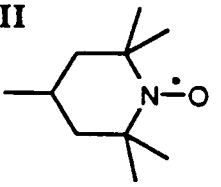

B R = 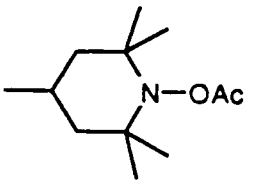

C R = Me

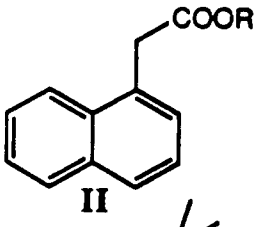

II

II A R = 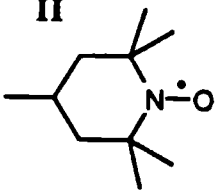

B R = 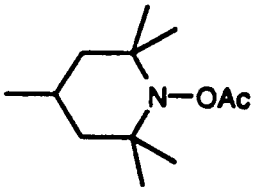

C R = Me

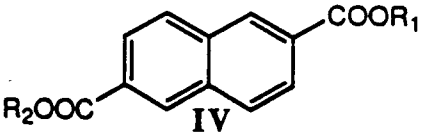

IV

IV A R_1 = 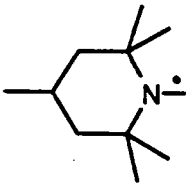

, R_2 = H

B R_1 = 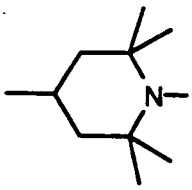

, R_2 = H

C R_1 = Me, R_2 = H

D R_1, R_2 = 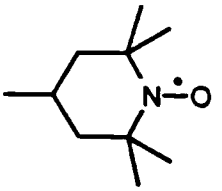

E R_1, R_2 = 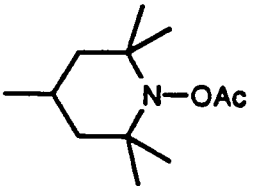

F R_1 = Me, R_2 = Me

Fig. 2, Green, et al

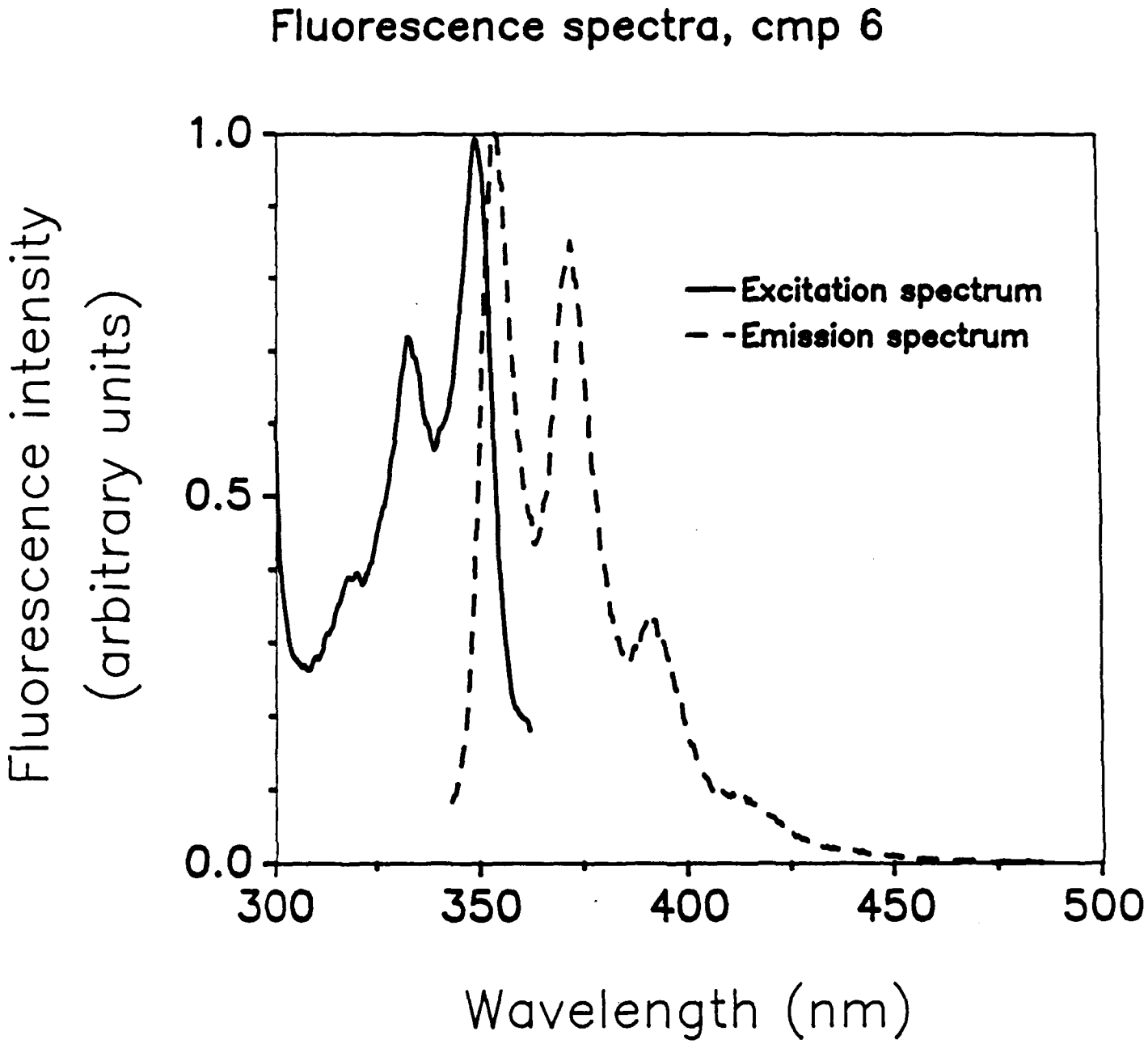

Fig. 3, Green, et

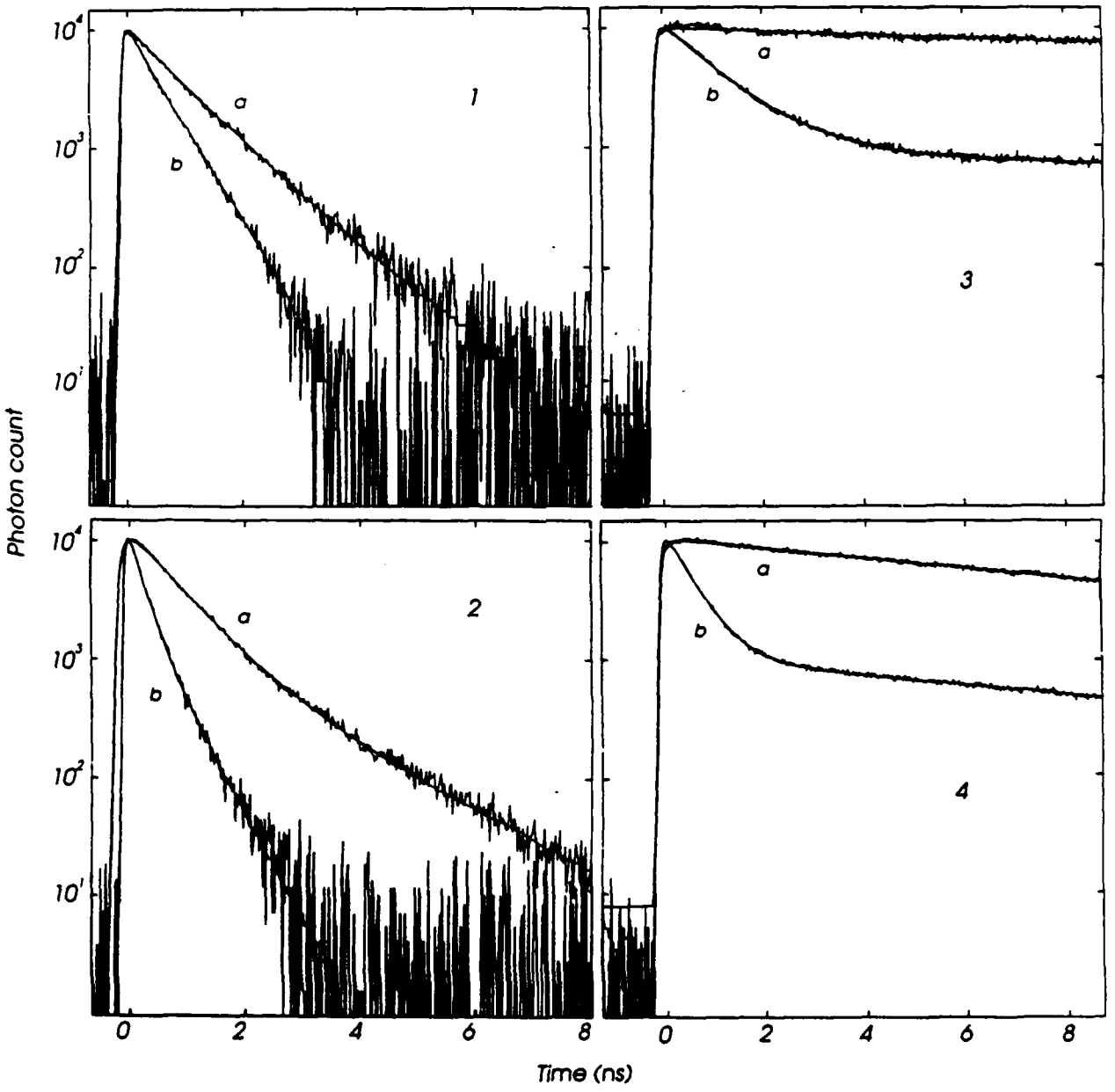

fig. 4, Green, et a

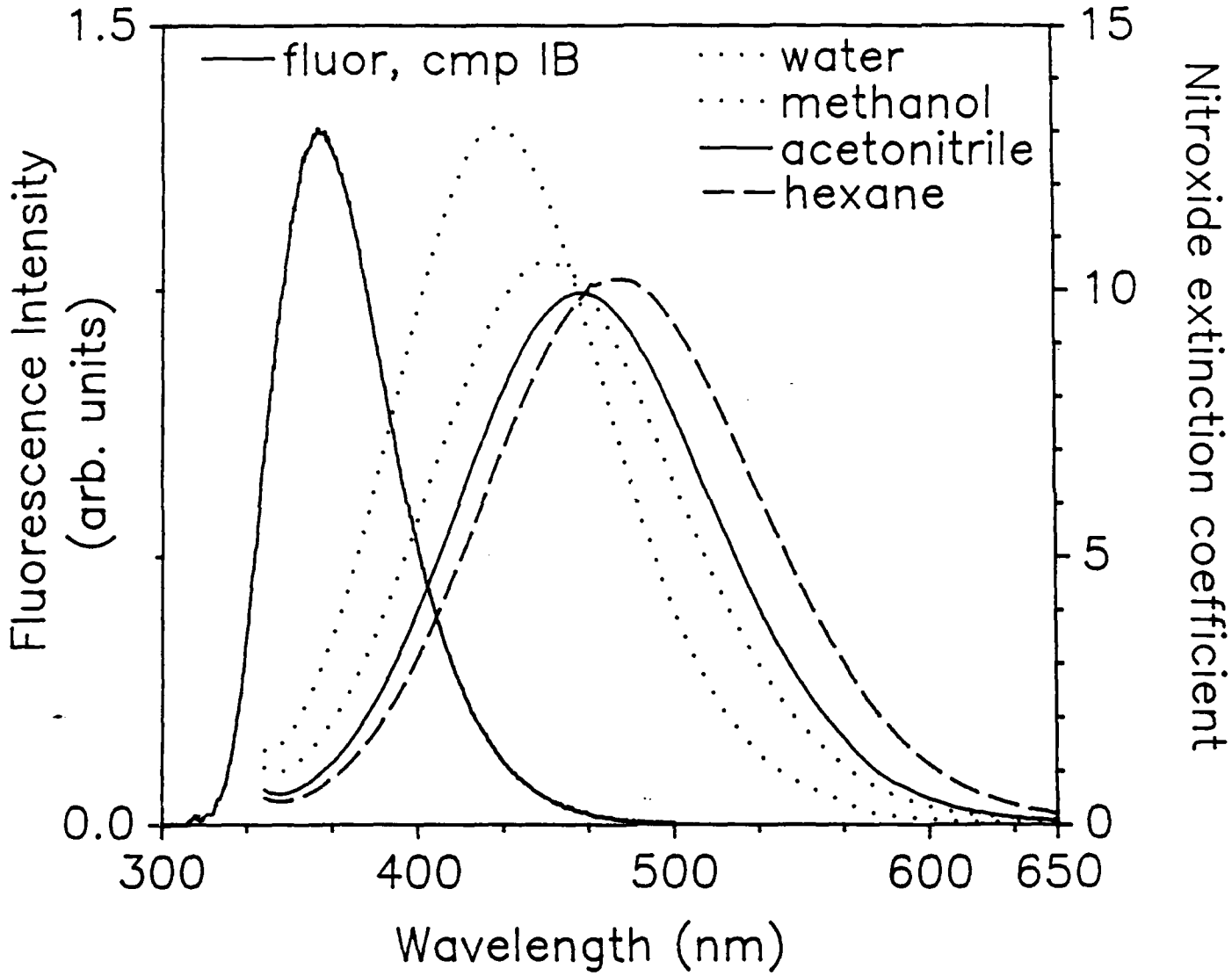

Fig. 5, Green

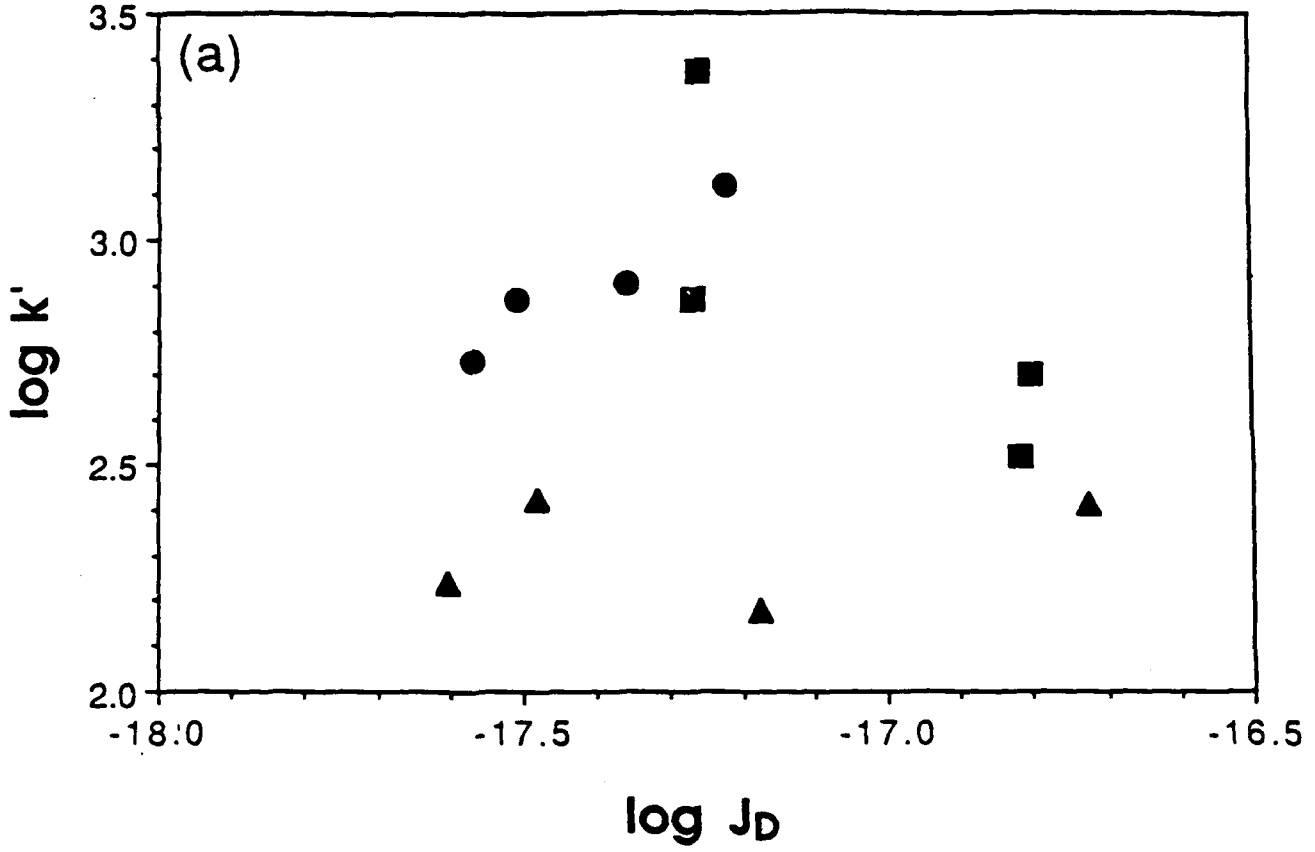
(a)
3.5
3.0
2.5
2.0
log k'
-18.0
-17.5
-17.0
-16.5
log J_D

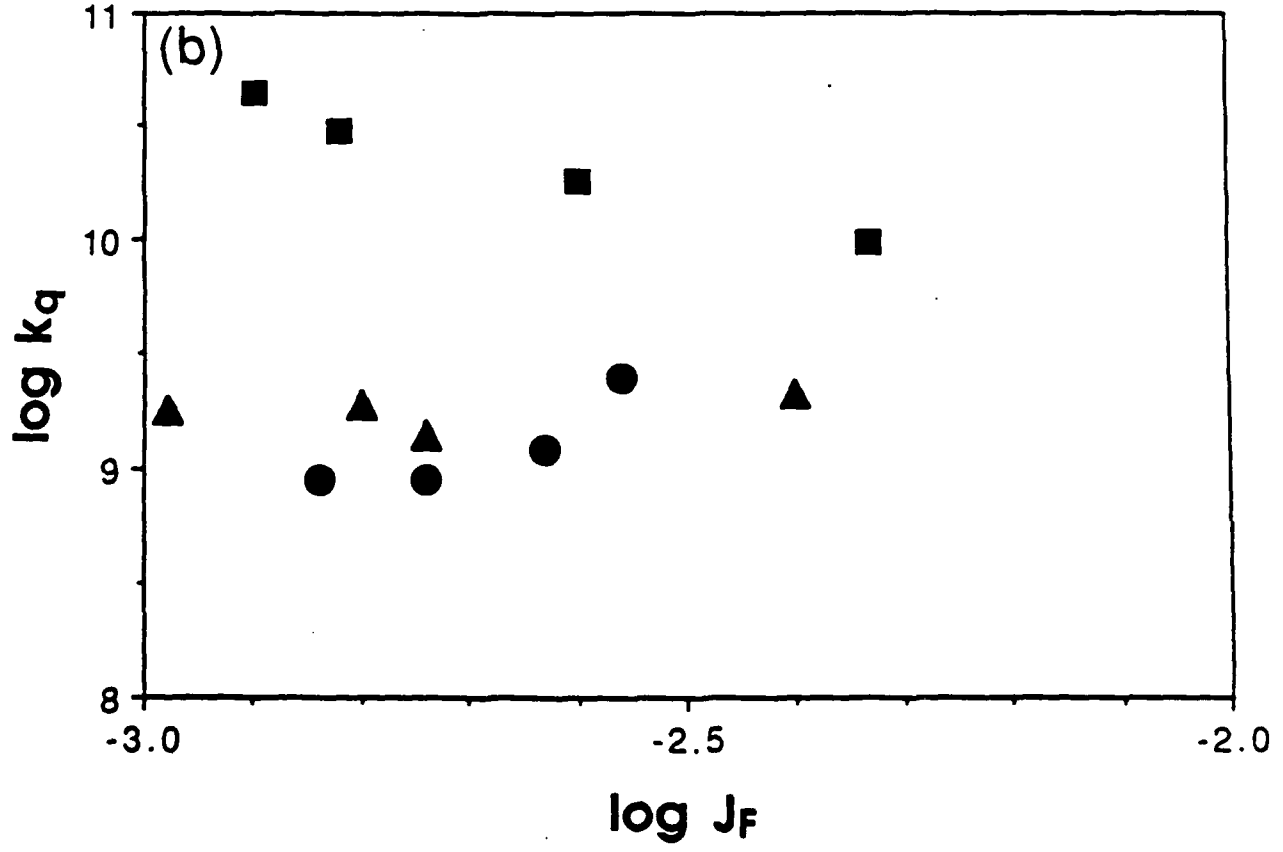
(b)
11
10
9
8
log k_q
-3.0
-2.5
-2.0
log J_F

fig. 6, Green, et.

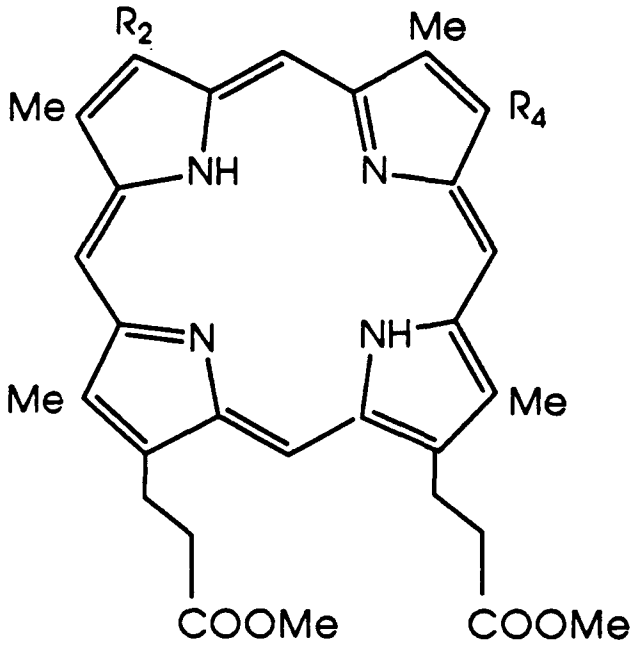

V A and B

R_2 (R_4) =

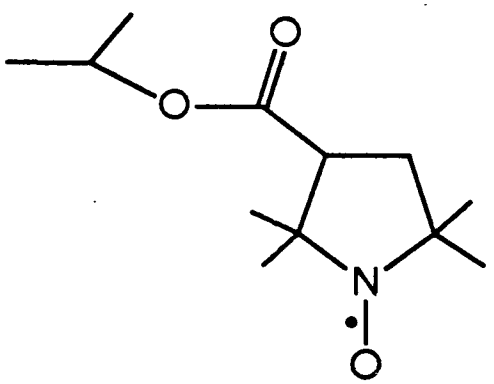

R_4 (R_2) = CH_2CH_3

C

R_2 (R_4) = CH_2CH_3

R_4 (R_2) = $CHOHCH_3$

Fig. 7, Green, et al.

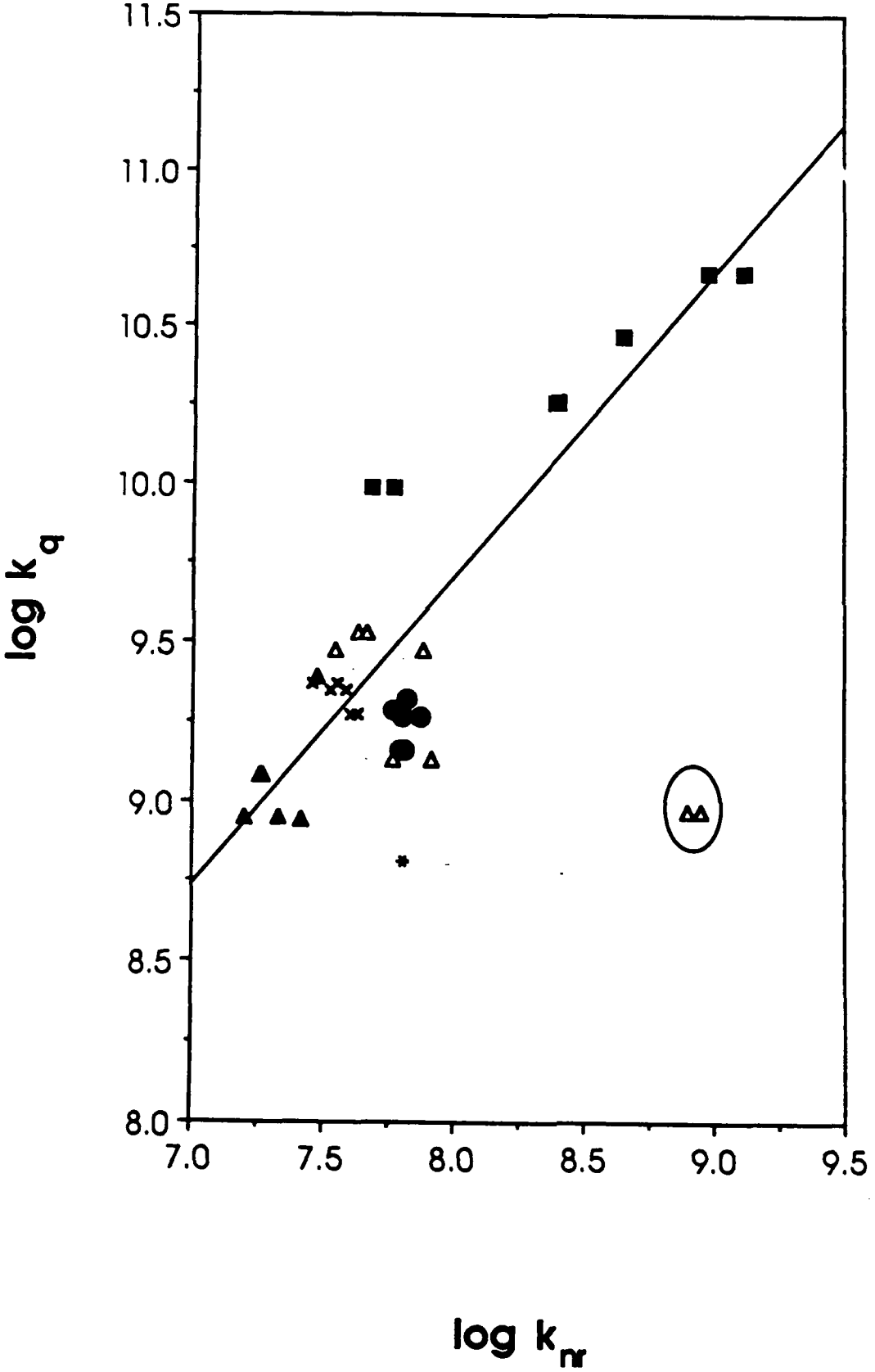

Fig. 8, Green et al

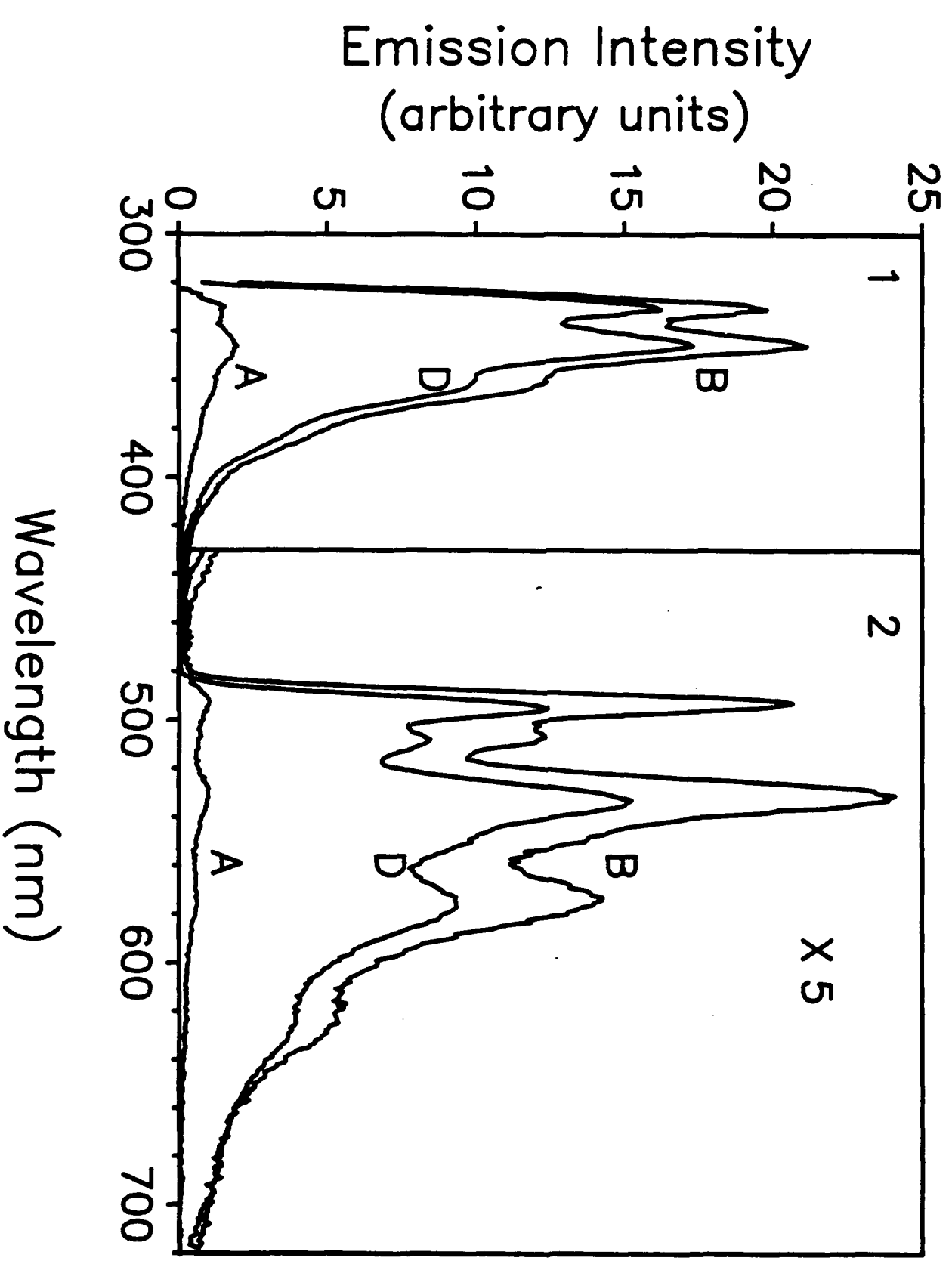

rev 1-31-90

Polarized Electronic Spectra of Z-DNA Single Crystals

Pui S. Ho and Guangwen Zhou

Department of Biochemistry and Biophysics

Oregon State University

Corvallis, OR 97331

and

Leigh B. Clark*

Department of Chemistry

University of California, San Diego

La Jolla, California 92093-0342

Synopsis

Polarized electronic absorption spectra of the (100) face of single crystals of the Z-form double helical duplex of d(m^5CGUAm^5CG) have been obtained from Kramers-Kronig analysis of reflection data. The *c* crystallographic axis is parallel to the helix axis and shows but weak absorption. The *b* axis is perpendicular to the helix axis and shows a structureless absorption band centered at 270 nm with an oscillator strength of 0.26. Calculations of the crystal spectra utilizing available transition moment data for the individual chromophores are carried through using the oriented gas model (no interbase interactions) and, again, employing all base-base interactions (point dipole) in the duplex. The calculated hypochromism of the 270 nm band is much less than the experimental value obtained from the crystal data. The crystal spectra appear to be representative of Z-form double helices of essentially infinite length and not of a collection of twelve base duplexes. No evidence for $n\pi^*$ transitions polarized parallel to the helix axis is found.

INTRODUCTION

At the simplest level of interpretation, the electronic absorption spectrum of a polynucleotide is just a summation of the absorption spectra of the individual chromophores that are present. Refinements bring changes owing to differences in the environment of the chromophores and, as a separate issue, chromophore-chromophore interactions (both base stacking and pairing). These effects lead to conformationally dependent changes in the optical properties of solutions of polynucleotides of all strandedness. The hypochromism of native DNA and other stacked polynucleotides relative to unstacked or random coil arrangements is routinely used to assay the amount of order present.[1] More recently the observation that Z-form DNA exhibits less integrated absorption in the 260 nm region than even the B-form has been used to study various aspects of Z-B transformations.[2] Although there is overall hypochromism exhibited by the 260 nm absorption band in the B to Z transition there is in fact pronounced hyperchromicity in the long wavelength edge (~295 nm).

The absorption curves of isotropic solutions are of course a spherical average of all orientations of the statistical distribution of conformations present, and since the broad, diffuse bands resulting from the several transitions of the individual chromophores are substantially overlapped, little detailed electronic spectral information is available from solution absorption spectra. Considerable effort has been applied to the measurement and interpretation of CD spectra in order to elucidate the structure and conformation of polynucleotides. Although CD spectra are very sensitive to conformation and contain the extra dimension of the sign of the CD bands, it is still not a straightforward matter to use CD data to gain specific information regarding the effects of base pairing and stacking. Linear dichroism (both flow- and electric field-induced) studies are useful in identifying the strength of absorption parallel and transverse to the helical axis, but necessary estimates concerning the extent of order tend to limit the results quantitatively, and, at best there is still a random distribution about the orientation axis.

Recent advances in the crystallography of oligonucleotide single crystals affords us the opportunity to examine anisotropies that may exist in the absorption tensor of these polymers by studying the polarized electronic spectra of such crystals. It may then be possible to relate observed anisotropies to specific conformations, base sequences and interactions and to provide a useful test for the theories dealing with the optical properties of polynucleotides. We hope that the present work on perfectly ordered systems (*viz.* crystals) will complement the other experimental approaches mentioned above.

In this paper we report polarized UV spectra taken from the *bc* face of a single crystal of the Z-form d(m^5CGUAm^5CG)·d(m^5CGUAm^5CG) duplex. Since the *c* crystallographic axis coincides with the helix axis, we obtain a spectrum for radiation polarized parallel to the helix axis and another spectrum for radiation polarized perpendicular to the helix axis. The latter spectrum (*b*-axis polarized) represents the transitions of the duplex as they project onto the *b* axis and may be different from the corresponding projections onto the *a* crystallographic axis. It is just such a difference that we would ultimately hope to exploit when the *a* axis spectrum becomes available. For comparison we report spectra for all three crystal axes that are calculated

from the known spectral parameters of the purine and pyrimidine chromophores using an oriented gas approach (no interactions or mixing) and a point dipole treatment including all base-base interactions of the twelve member duplex.

Crystal Structure

Single crystals of the self-complementary d(m^5CGUAm^5CG) oligomer are of orthorhombic space group $P2_12_12_1$ and have unit cell dimensions a = 17.52 Å, b = 30.44 Å and c = 44.82 Å.[3] There are four duplexes of the Z-conformation per unit cell. Duplexes pack end-to-end not only as pairs in a given unit cell but in adjacent cells in such a way as to create uniformly continuous, parallel strands of Z-DNA with the helix axis parallel to the crystallographic *c* axis. Each duplex makes one-half turn of the helix. Figure 1 shows a projection of six (stick model) duplexes onto the *bc* face. The duplex at site 2 ($\bar{x}$ + 1/2, −y, z + 1/2) continues the half helix of site 1 (x,y,z) to form one full turn of the helix in one unit cell. Projections of the remaining two duplexes of the unit cell at site 3 ($\bar{x}$, y + 1/2, $\bar{z}$ + 1/2) and site 4 (x + 1/2, $\bar{y}$ + 1/2, $\bar{z}$) are obtained from sites 1 and 2 by a translation and then a 180° rotation around an axis parallel to *b* (two-fold screw). Thus, the transition moment of a particular band of any given residue at all four unit cell sites project equivalently (except for phase) onto the three crystallographic axes. Since observed absorption is proportional to the square of these projections, all four duplex sites therefore are spectroscopically equivalent when viewed along any unit cell axis. The normals to the planes of the bases are pitched at an average of 8° from the *c* axis. The direction cosines of these normals and the C_4–C_5 reference axis of the purines and the N_1–C_4 reference axis of the pyrimidines for the twelve sites are given in Table I. The attitudes of all the bases in the structure are completely specified by the values given in Table I.

Another presentation of the crystal structure is shown in Fig. 2, where the atoms are drawn with their van der Waal's surfaces. The heavy solid lines connect the phosphorus atoms of the phosphate backbone. The packing of the duplexes into continuous helical strands with no "gaps" is apparent in this figure. Crystals were grown by a vapor diffusion method that will be described elsewhere.[3] Relatively large crystal faces (~200 μ) are needed for the spectral

measurements, and crystals of this size were occasionally obtained. The general morphology is given in Fig. 3. The crystals are pseudohexagonal and elongated along *c*. The principal faces are (100), (001) and (110).

Spectra

Owing to the orthorhombic crystal symmetry, the *bc* crystal face will show two "independent" absorption spectra. These spectra correspond to the incident radiation polarized parallel to the *b* axis and parallel to the *c* axis and will sample transitions to B_2 and B_1 crystal factor group states respectively. Radiation polarized at intermediate angles will simply be a cosine squared weighted average of the *b* axis and *c* axis spectra. Based on general considerations of the nature of the electronic spectra of the purine and pyrimidine chromophores one expects relatively strong absorption polarized perpendicular to the helix axis ($\pi \rightarrow \pi^*$, in-plane polarized) and about 10 to 100 times less absorption polarized parallel to the helix axis (*vide infra*). The molar concentration of base chromophore is 3.30 moles per liter in the crystal, and assuming an extinction coefficient of the order of 10^4 cm^{-1} M^{-1} one can calculate a maximum path length limitation for a maximum practical absorbance value of 3 to be about 10^{-4} cm. Crystals of these oligomer duplexes are "blocky" in nature, and direct absorption experiments with micron sized crystals would be very difficult at best. In order to avoid the thin crystal requirement of direct absorption measurements, we have measured the polarized reflection spectra from the *bc* crystal face of relatively large single crystals (~200 μ). The corresponding absorption curves are subsequently obtained by Kramers-Kronig analysis of the reflection data. The instrument used and the transformation procedure have been described in other publications.[4] A 15× Cassegrainian reflective microscope objective is used to focus the incident radiation onto the crystal face. The incident beam is sharply tailored to minimize depolarization effects and to reduce the convergent nature of the focused light to an average angle of 1° from normal incidence. A 100 × 200 micron image of the monochromator slit is formed on the crystal surface. The dimensions of the crystal face must be somewhat larger than that image.

For the spectral measurements the crystals were mounted on a small pedestal inside a delrin capsule which incorporated a demountable window. A small drop of mother liquor (50:50 water:2-methyl-2,4-pentadiol) was used to adhere the crystal to the pedestal. Additional drops of mother liquor were placed inside the capsule to maintain a saturated atmosphere around the crystal. The capsule was attached to a goniometer head and the crystal face brought normal to the incident light beam. The whole assembly was rotated about an axis colinear with the incident light so as to align the chosen crystal axis with the polarization of the light beam. Finally, the window was removed, the alignment readjusted as needed and the reflection spectrum scanned from 370 to 190 nm. The crystal was subjected to the "drying" effects of the laboratory air for about 40 minutes. No degradation was observed, however, during the course of the 40 minutes nor during a similar measurement period on a subsequent day about two months later.

The reflection spectra of the *bc* face are shown in Fig. 4. For such small crystals (~0.1 mm thick) mounted with the backside in contact with a film of mother liquor, one would expect there would be "extra" reflections that add to the signal throughout the transparent region. The extra reflections arise from the crystal/mother liquor boundary and the mother liquor/delrin (pedestal) boundary. These additional reflections are of small magnitude relative to the reflection from the air/crystal boundary (front surface) because the indices of refraction of crystal, mother liquor and delrin are similar in magnitude. However, upon the onset of absorption in the crystal, virtually no light manages to penetrate as far as the back surface of the crystal, and the extra contributions vanish. The dashed extensions of the reflectivity curves in Fig. 4 represent our attempt to remove these unwanted reflections. The onset of absorption in these crystals is near 310 nm and the extensions were drawn to smoothly connect with the curves at the point where only the front crystal surface contributes to the signal. The use of the correct reflectivity in the transparent region leading up to the onset of absorption is important in the Kramers-Kronig procedure, for it is the calculated outcome in this region that is used as a criterion for the adequacy of the transformation. The transformation involves numerical integrations over the entire frequency domain

(0→∞), whereas measurements are made over a "somewhat" narrower region (370-190 nm). The usual procedure is first to extend the measured spectrum with trial reflectivities on the red side (to zero frequency) and in the vacuum UV (to very large but finite frequency).[4] Then these extensions are adjusted in a systematic way until zero absorption is calculated throughout the known transparent region. The result is not unique and depends on the particular shape assumed for the adjacent region in the vacuum UV. By employing a variety of vacuum UV extensions a family of absorption curves can be obtained that mutually satisfy the transparent region constraint. The derived absorption spectra are shown in Fig. 5. The range of values for the computed extinction coefficients that arises from the various vacuum UV trial functions are indicated by the widening fans. The curves show broad, diffuse bands with no apparent structure.

The removal of the unwanted extra reflection in the transparent region (the dashed extensions of Fig. 4) is warranted for two reasons. First, different crystals show different magnitudes of extra reflection, however in all cases the effect disappears at 310 nm. Second, the raw data, i.e. the uncorrected reflection curve, cannot be satisfactorily transformed. The step in the reflection at 320 nm always results in an absorption spectrum with a negative dip at 370 nm and a positive peak at 323 nm. Our experience over some years with the Kramers-Kronig transformation of reflection data leads us to assert that a satisfactory transform cannot be obtained from a reflection spectrum that has an incorrect shape. We conclude that the low energy extensions shown in Fig. 4 are appropriate.

The most likely source of error in the computed extinction coefficients, in our estimate, arises from imperfections on the crystal surface. Surface imperfections tend to scatter the incident radiation and uniformly lower the reflected signal. Again, our experience with the Kramers-Kronig analysis of reflection data, suggests that a given uniform percentage lowering of the reflection produces an equivalent percentage error in the computed absorption spectrum. The correct shape is, however, maintained. The crystal surfaces used in this study showed regions that were smooth and shiny under microscopic examination. Although these regions ought to have yielded proper reflectivity, no independent check of the accuracy of the reflection

coefficients was available.

Interpretation

For our purposes here we will assume that the purine and pyrimidine bases are the only chromophores that directly contribute to the absorption at wavelengths greater than 190 nm. The deoxyribose moieties, the phosphate linkages, as well as the water molecules present in the structure are not expected to absorb at wavelengths longer than about 180 nm. The excited electronic states of the individual bases are now known fairly well (*vide infra*) and conform with the expectations of basic π electron theory. The strongest bands ($\varepsilon_{ave} \approx 10^4\ cm^{-1}\ M^{-1}$) are assigned to $\pi \rightarrow \pi^*$ transitions and are all polarized in the molecular plane. $n \rightarrow \pi^*$ bands are expected to be polarized normal to the planes of the bases, but little evidence for this type of transition has been found. Any such bands, if present, ought to be weak and presumably are lost beneath the much stronger in-plane polarized bands.

On the other hand the model for an electronic band as being represented by a single transition moment direction is an approximation. Through vibrational distortions the individual vibronic transitions may appear with different polarizations. Those that remain polarized in-plane will appear with slightly varying in-plane directions; they should, however, cluster around some dominant direction. Some vibrational distortions lead to "forbidden components" polarized normal to the molecular plane. The result is that even a nominally in-plane polarized $\pi \rightarrow \pi^*$ transition can be expected to show some out-of-plane transition probability. Transition moment data acquired from spectral measurements on single crystals of individual bases suggest that 3-5% of a nominally in-plane polarized intensity can be expected to appear polarized normal to the molecular plane.[4-6]

Returning to the crystal absorption spectra for the 37,000 cm^{-1} (270 nm) band we see the *b* axis spectrum (i.e. close to parallel to the planes of the bases) shows an absorptivity of 9,100 $cm^{-1}\ M^{-1}$ whereas the ||*c* spectrum exhibits a corresponding value of about 500. The component oscillator strengths evaluated with the formula $f = 4.32 \times 10^{-5} \int \varepsilon\, d\, \bar{\nu}$ where ε is the decadic molar extinction coefficient and $\bar{\nu}$ is the frequency in cm^{-1} are 0.26 and 0.017 for the *b*-axis and

c-axis, respectively. The oscillator strength appearing in the *c*-direction is about three times larger than would be anticipated if it arose solely from the 8° cant of in-plane transition moments of the bases. The difference along *c* corresponds to a few percent of the in-plane intensity and, as discussed above, likely corresponds to the out-of-plane components of the nominally in-plane polarized π-π* transitions rather than perpendicularly polarized nπ* bands. In any event, the dichroic ratio is fairly large, $(f_b/f_c) = 15$. Given all the above considerations we see that the experimental spectra conform to expectations in their general appearance.

Model Calculations

Here we will calculate the spectrum of the duplex from known monomer transition properties and the known relative positions and orientations of the bases in the crystal. The simplest approach involves treating the duplex as an "oriented gas" of twelve bases each of which will be carrying its personal load of electronic transitions. Each transition moment is projected onto the *a*, *b* and *c* crystal axes and the component oscillator strength then computed. For comparison to experimental crystal spectra the individual components bands are converted to Gaussian shaped bands using a half-width that is common to various crystal spectra of the individual bases (4,500 cm^{-1}) and then summed to yield the final computed absorption spectra. For comparison to random solution spectra the transition moment data are used directly to compute a summed Gaussian spectrum.

The optical effects of base-base interactions can be handled most simply using an Independent Systems or Exciton Model approach and employing the point dipole approximation to evaluate interaction terms. Conventional wisdom suggests that the point dipole approximation is not adequate for the nearest neighbor interactions along a polymer chain and that distributed monopoles (or higher multipoles) ought to be used.[7] The trouble in this regard is that the monopole distribution for each transition must be obtained from LCAO wave functions of dubious trustworthiness. At the present time, there is no satisfactory assignment of the experimentally observed monomer transitions according to any of the various LCAO quantum mechanical results.[8] Treating the interactions in the point dipole approximation using all experimentally

determined transition moment directions seems to be an appropriate compromise to take at the present time. The excited state eigenfunctions of the duplex are obtained as linear combinations of all monomer excited states by diagonalizing a Hamiltonian matrix whose off diagonal elements are mathematically equivalent to the electrostatic interaction of the two transition moment dipoles from the ground state to the states involved in that matrix element. These terms are given by the usual expression

$$h_{i\alpha,j\beta} = (1 - \delta_{ij}) \left[d_{i\alpha} \cdot d_{j\beta} - 3 \cos (d_{i\alpha} \cdot \hat{r}_{ij}) (d_{j\beta} \cdot \hat{r}_{ij}) \right] / (|r_{ij}|)^3$$

where α and β are the transitions on sites i and j respectively. The **d**'s are transition moment vectors and $\mathbf{r}_{ij}$ is the vector between the respective base centers (i→j). The Kronecker delta, δ_{ij}, eliminates terms between transitions at the same site, and diagonal terms, $h_{i\alpha,i\alpha}$ are just the unperturbed transition energies. New (perturbed) transition moment vectors are evaluated from the resultant eigenfunctions and projected individually onto the *a*, *b* and *c* crystal axes at their computed new energies. The results are again Gaussianized and finally presented as spectral curves appropriate for *a*, *b*, *c* crystal axis spectra. There are 74 transitions covering a range from 33,000 to 74,000 cm^{-1} (300-135 nm) to be included in the twelve bases of the duplex so that the matrix to be diagonalized is 74 × 74. Gaussianizing the output seems an appropriate tack to take in presenting and comparing these calculated results owing to the complexity of the assembly and the large number of overlapping transitions that must be dealt with.

Transition moment data for the individual transitions of the four bases have been obtained mostly from single crystal spectra of the bases (or various methylated forms).[4,5,9–12] We summarize these data in Table II. In certain higher energy cases an ambiguity remains in the crystal result and the choices excluded in the calculations reported here are indicated by parentheses. For this reason, the calculated spectra in the 210-190 nm region are presented provisionally. Band contours in this wavelength region do depend on the various choices possible, particularly for the fourth cytosine transition. In order to proceed in a consistent manner we have also used transition energies taken from crystal spectra. The transition energy differences between solution

and crystal environments is usually *not* large in any event. With the possible exception of the 46,000 cm^{-1} (217 nm) band of the uracil chromophore, no perpendicularly polarized transition has been observed with any certainty. Most of the perpendicularly polarized intensity observed in crystal spectra is more likely to be simply "forbidden" components of the nominally in-plane polarized transitions.

The results of the calculations for the *a*, *b* and *c* axes are presented in Fig. 6 along with the experimental spectra for comparison. Both schemes (i.e. oriented gas and with interactions) predict noticeable differences in the curves along the *a* and *b* axes particularly in the 210-190 nm range. The first band maximum appears at 265 nm along *b* and at 261 nm along *a* in the oriented gas analysis. After base-base interactions are included there is a slight blue shift of the peak position of the *a* axis spectrum (to 259 nm) and an even smaller red shift along the *b*-axis. These changes ought not be considered only as shifts of energy levels but also as resulting from the redistribution of intensity among the multitude of closely spaced (overlapped) transitions.

The theory of the hypochromic effect in stacked polynucleotides was worked out by Tinoco[13,14] and by Rhodes.[15] The in-plane transition moments of an approximately card-pack stack of bases mix under their mutual interactions so as to shift intensity from lower energy states to higher energy states. Transition moments polarized normal to the planar bases show the opposite effect (hyperchromism) owing to their approximate head-to-tail arrangement. Model calculations in the point dipole approximation presented by both Tinoco and Rhodes in the early work were done with assumed, artificial transition moment data, and the results were simply shown to be consistent with the observed sign and general magnitude of the observed effects. More recent work by Rizzo and Schellman,[7] for example, use a mix of theoretical and empirical parameters for the monomer transition moment data set. To our knowledge, however, there has been no hypochromism calculation at any level of approximation in which only experimental transition moment data is used and that brings out the spatial anisotropy of the duplex. The calculations reported here pertain to incident light polarized along the *a*, *b* and *c* crystal axes of the duplex, and since the spectral properties are not the same in these different directions, the results

contain more verifiable information than the outcome of isotropic calculations. Of course, for comparison to isotropic solution spectra the calculated results can be randomized by summing the *a*, *b* and *c* axis spectra and dividing by 3.

The calculated curves shown in Fig. 6 give 18%, 16% and 6% reductions in oscillator strength along the *a*, *b* and *c* crystal axes respectively for the 260 nm region. Only the experimental *b*-axis result is available for comparison to its corresponding calculated value, and here the observed loss of absorption of 45% corresponds to about 2.8× more reduction than that calculated. Along both *a* and *b* axes there is calculated hypochromicity throughout the low energy region, while the higher energy region (220-180 nm) shows mixed hypo/hyperchromicity. Although not apparent in Fig. 6, the very weak absorption intensity polarized parallel to the helix axis shows a slight decrease in f number for the low energy region arising from base-base interactions. This result occurs since the parallel spectrum arises simply as the components of the in-plane polarized transitions that are undergoing hypochromic changes.

In order to investigate the difference between the theoretical and experimental results for the *b*-axis hypochromism we compare in Fig. 7 the randomized crystal spectrum to the aqueous solution spectrum of an equivalent mix of the constituent deoxynucleosides. Although the curve derived for the randomized crystal spectrum using the oriented gas approach differs in shape somewhat from that of the nucleoside mix, the oscillator strengths differ by only 7% ($f_{260} = 0.32$ for the mix and 0.30 for randomized oriented gas). The comparison is judged reasonable considering the transition moment data are taken from various related purine and pyrimidine bases and not the specific deoxynucleosides present. Since there are twelve base pairs per helical turn one might guess the *a* and *b* axes to show similar spectra, and this supposition is supported by the calculations which yield only ~9% more intensity along *a* than along *b* and similar values for the calculated hypochromism. Assuming such rough isotropy is the case, we can (in the absence of experimental *a* axis data) construct an approximate randomized crystal spectrum by taking twice the *b* axis spectrum, adding the *c* axis spectrum and dividing by 3. The result is a curve where $\lambda_{max} = 270$ nm, $\varepsilon_{max} = 6{,}200\ cm^{-1}\ M^{-1}$ and f (isotropic) = 0.18. The last two numbers may be

~5% low judging from the 9% more absorption predicted along the *a* axis compared to the *b*-axis. The isotropic hypochromism [$H = (1 - f_{stacked}/f_{unstacked})$] of the long wavelength band upon including base-base interactions is 0.17, whereas the approximate isotropic spectrum derived from the crystal data gives a value of H = 0.45 (in comparison to the mix of deoxynucleosides).

As mentioned earlier, surface imperfections may contribute to the measured hypochromism. However, another source of the above difference in H may arise in chain length considerations. It must be recognized that the stacking arrangement of duplexes in the crystal generates essentially continuous double helical chains, whereas the calculations include only the interactions within a single duplex. A more appropriate comparison for these calculated results would seem, therefore, to be with solution spectra of the duplex itself. Fig. 8 shows the aqueous solution spectra of the melted form (80°C) and both B and Z double helical forms. Relative to the melted curve the 260 nm band exhibits a value of H = 0.19 for the Z-form, and this value compares reasonably with the calculated result of 0.15. Such agreement tends to support the assertions that (i) the crystal spectra pertain to essentially infinite helices and (ii) the calculation of the absorptive properties of polynucleotides may be adequately approached within the framework of the point dipole approximation. The calculations we have done lead to no hyperchromicity in the long wavelength region (~295 nm), whereas such is observed. Perpendicularly polarized, $n\pi^*$ intensity has been presumed to provide the mechanism for this effect. However, our calculations included no such transition in the long wavelength region. The weakness of the experimental absorption polarized parallel to the helix axis (*c* crystal axis) rules out the $n\pi^*$ mechanism for the hyperchromicity in the long wavelength region.

SUMMARY

Absorption spectra of the *bc* crystal face of single crystals of the Z-form duplex d(m^5CGUAm^5CG)·d(m^5CGUAm^5CG) have been obtained from polarized reflection data. The crystal structure is such that the results are appropriate for an infinite, Z-form double helix with a repeating unit of two six base-pair duplexes. The *c* axis spectrum is parallel to the helix axis and shows very small absorption intensity, whereas the *b*-axis spectrum is perpendicular to the helix

axis and shows the $\pi\pi^*$ base transitions strongly.

Calculations based on both an oriented gas model and a point dipole interaction model suggest that the *ab* crystal face (i.e. perpendicular to the helix axis) will show significant differences between the *a* and *b* axis spectra. The results for the dipole interaction model lead to a hypochromism of 0.15 compared to an experimental value of 0.45. The disparity is most likely attributable to the chain length differences between the crystal (infinite) and duplex (six-mer). Efforts at preparing crystals with (*ab*) faces large enough for measurement and extending the spectra deeper into the vacuum UV are presently underway.

*This work was supported by grants from the NIH (#GM38575 to L.B.C.), NIEHS (#E500210 to P.S.H.) and ONR (#N00014-88-K-0388 to P.S.H.).

References

1. See for example Cantor, C.R., & Schimmel, P.R. (1980) *Biophysical Chemistry*, **Part II**, W.H. Freeman & Co., New York.
2. Chaires, J.B., & Norcum, M.T. (1988) *J. Biomol. Struc. Dyn.* **5**, 1187.
3. Zhou, G., & Ho, P.S. (1989) in preparation.
4. Zaloudek, F., Novros, J.S., & Clark, L.B. (1985) *J. Chem. Chem. Soc.* **107**, 7344.
5. Novros, J.S., & Clark, L.B. (1986) *J. Chem. Phys.* **90**, 5666.
6. Clark, L.B. (1986) *J. Am. Chem. Soc.* **108**, 5109.
7. Rizzo, V., & Schellman, J.A. (1984) *Biopolymers* **23**, 435.
8. Callis, P.R. (1986) *Photochem. Photobiol.* **44**, 315.
9. Eaton, W.A., & Lewis, T.P. (1970) *J. Chem. Phys.* **53**, 2164.
10. Clark, L.B. (1977) *J. Am. Chem. Soc.* **99**, 3934.
11. Clark, L.B. (1989) *J. Phys. Chem.* **93**, 5345.
12. Clark, L.B. (1990) *J. Phys. Chem.* **94**, April, in press.
13. Tinoco, I., Jr. (1960) *J. Am. Chem. Soc.* **82**, 4785.
14. Tinoco, I., Jr. (1961) *J. Am. Chem. Soc.* **83**, 5047.
15. Rhodes, W. (1962) *J. Am. Chem. Soc.* **83**, 3609.
16. Clark, L.B. (1989) *J. Phys. Chem.* **93**, 5345.
17. Novros, J. (1971) Ph.D. Thesis, University of California, San Diego.
18. Edmondson, S.P., & Johnson, W.C. Jr. (1986) *Biopolymers* **25**, 2335.
19. Edmondson, S.P., & Johnson, W.C. Jr. (1985) *Biopolymers* **24**, 825.
20. Matsuoka, T., & Norden, B. (1982) *J. Phys. Chem.* **86**, 1378.

TABLE I

Coordinates of Molecule Centers and Direction Cosines of the Reference Axes and Normals to the Planes

	Center[a]			Reference Axis[b]			Normal[b]		
	a	b	c	a	b	c	a	b	c
C1	0.6847	0.3769	-0.0765	0.5728	-0.8139	-0.0973	0.1486	-0.0136	0.9888
G2	0.4368	0.4481	0.0179	0.0619	-0.9948	0.0805	0.0540	0.0839	0.9950
U3	0.5540	0.4986	0.0938	-0.4433	-0.8963	0.0147	0.0389	-0.0029	0.9992
A4	0.5245	0.6505	0.1771	-0.8254	-0.5594	-0.0753	-0.0862	-0.0069	0.9963
C5	0.6102	0.6101	0.2581	-0.9904	-0.1261	-0.0572	-0.0482	-0.0734	0.9961
G6	0.8292	0.6962	0.3429	-0.8760	0.4810	-0.0349	-0.0538	-0.0256	0.9982
C7	0.5524	0.5575	0.3310	-0.1438	0.9868	0.0741	0.0899	0.0876	-0.9921
G8	0.4574	0.4126	0.2438	-0.6699	0.7423	-0.0168	0.0445	0.0176	-0.9989
U9	0.6065	0.4390	0.1669	-0.9480	0.3153	0.0427	-0.0110	0.1017	-0.9948
A10	0.7570	0.3220	0.0822	-0.9585	-0.2635	0.1086	-0.0912	-0.0775	-0.9928
C11	0.7826	0.3779	-0.0024	-0.7854	-0.6083	0.1146	-0.1810	0.0486	-0.9823
G12	1.0520	0.3958	-0.0886	-0.3025	-0.9530	0.0133	0.0111	-0.0175	-0.9998

[a]The centers of the cytosine and uracil residues were taken as the midpoint between the N_1 and C_4 line segment while the midpoint of the C_4–C_5 bond was taken as the center of the guanine and adenine residues. These coordinates are given as fractions of the unit cell dimensions.

[b] The reference axis is the C_4–C_5 line in the purines and the N_1–C_4 line in the pyrimidines. The normal was constructed by taking the vector product of the reference axis vector with the vector directed from C_4 to C_2 in the purines and N_1 to C_2 in the pyrimidines.

TABLE II

Monomer Transition Moment Data

		ν^a (cm^{-1})	λ (nm)	f	μ (Å)	θ^b	Ref
Adenine	1	38,500	260	0.11	0.513	83	16
	2	37,500	267	0.20	0.701	25	
	3	47,000	213	0.25	0.700	-45	
	4	49,000	204	0.11	0.455	15	
	5	53,700	186	0.30	0.718	72	12
	6	56,000	179	0.10	0.406	-45	
	7	62,500	160	0.23	0.582	6	
	8	69,900	143	0.10	0.363	-45	
Cytosine	1	36,900	271	0.14	0.591	6	
	2	43,000	233	0.03	0.254	-35	
	3	44,600	224	0.13	0.518	76	4
	4	50,500	198	0.36	0.811	86 (-26)[c]	
	5	62,000	161	0.15	0.472	0 (60)	
	6	66,000	152	0.20	0.529	60 (0)	
Guanine	1	36,000	272	0.16	0.640	-4	
	2	39,400	254	0.25	0.765	-75	
	3	49,000	206	0.41	0.878	-71	10
	4	53,000	187	0.48	0.914	41	
	5	63,000	159	0.20	0.541	0 (40)	
	6	69,000	145	0.20	0.517	40 (0)	
Uracil	1	38,500	260	0.19	0.674	-9	9
	2	47,000	213	0.26	0.714	-53(+59)[d]	5
	3	46,000	217	0.007	0.118	⊥	
	4	55,000	182	0.31	0.721	-33(+39°)	17
	5	60,000	167	0.17	0.511	-40(+47)	

[a]Taken as peak positions in the crystal spectra of individual bases.

[b]In-plane transition moment directions using the Tinoco-DeVoe convention. For pyrimidines θ is positive toward N_3 from the N_1–C_4 reference axis, and for the purines θ is positive toward N_3 from the C_4–C_5 reference axis. Values in parentheses are alternate assignments owing to ambiguities in the crystal spectra of the particular base.

[c]The ambiguity in the polarization direction of transition 4 of cytosine has not been resolved. The +86° choice provides for a good fit of both CD and LD spectra of various G and C containing polymers, while the -26° choice does not lead to a satisfactory fit.[18] On the other hand, theoretical calculations uniformly predict values in the -35° to -45° range.[8]

[d]The ambiguity for band 2 had not been satisfactorily resolved. The -53° choice has been used to fit CD and LD spectra of polymers containing A and T.[19] On the other hand, theoretical calculations invariably yield values ~50°.[8] Additionally, the +59° direction harmonizes better with LD studies using stretched polyvinylalcohol sheets.

Figure Captions

Fig. 1. Projection of six duplexes onto the *bc* face. The helix axes are parallel to the *c* crystal axis. The four unit cell sites 1(x,y,z), $2(\bar{x}+\frac{1}{2}, \bar{y}, z+\frac{1}{2})$, $3(\bar{x},y+\frac{1}{2},\bar{z}+\frac{1}{2})$ and $4(x+\frac{1}{2},\bar{y}+\frac{1}{2},\bar{z})$ are indicated in the figure. The base numbering scheme runs 1 to 6 down one chain of m^5CGUAm^5CG and 7-12 up the complementary sequence of the duplex. The planes of the bases are tilted by an average 8° from the *ab* crystal plane.

Fig. 2. Projection onto the *bc* crystal plane using the van der Waal's surfaces of the atoms. The shaded duplexes are at the backside of the unit cell, whereas the unshaded duplex runs through the center of the unit cell. The continuous nature of the end-to-end stacking of duplexes is brought out in this figure. The solid lines connect the phosphorus atoms of the phosphate backbone. Atoms designations are as follows: closed concentric circles = carbon, dashed concentric circles = nitrogen, dotted concentric circles = oxygen, saw-toothed concentric circles - phosphorus.

Fig. 3. Crystal morphology of the Z-DNA duplex of d(m^5CGUAm^5CG). The *bc* face [with Miller indices (100)] was the face examined in this study. The dimensions are about $0.2 \times 0.2 \times 0.1$ mm.

Fig. 4. Reflection spectra for radiation polarized parallel to the *c* and *b* crystal axes. These axes are parallel and perpendicular to the helix axis respectively. The dashed portions are the extensions used in the transparent region for the Kramers-Kronig transformation procedure. These dashed extensions are drawn so as to eliminate "extra" reflection contributions from the back side of the crystal in the transparent region as discussed in the text.

Fig. 5. Absorption curves for the *b* and *c* axis derived from the reflection spectra shown in Fig. 4 by Kramers-Kronig analysis. The diverging width of the curves toward higher cm^{-1} correspond to the variations found for different trial vacuum UV reflectivities used in the transformation procedure. The "wiggles" arise from instrumental noise.

Fig. 6. Comparison of calculated and experimental crystal spectra. (Top) Calculated *a*-axis spectrum with (dots) and without (solid) interbase interactions. (Middle) Calculated *b*-axis spectrum with (dots) and without (solid) interbase interactions. The experimental *b*-axis curve from Fig. 5 is shown for comparison. (Bottom) The various curves are as above, but here represent the *c*-axis. Note the expanded vertical scale. Even on this scale the difference between the oriented gas and interactions models is not discernible.

Fig. 7. Comparison of isotropic or randomized spectra. The ordinate scale is on a per mole base chromophore basis. The solid curve (a) corresponds to the absorption spectrum of an equivalent mixture of the deoxynucleosides in aqueous solution. The dashed curve (c) represents the randomized spectrum of the transition moment data used for the four types of chromophores in the theoretical calculations and referred to as the oriented gas model approach in the text. The dotted curve is the randomized result after base-base interactions have been included. The solid curve was obtained from an equivalent mix of deoxynucleotides in neutral aqueous solution.

Fig. 8. Solution spectra of d(m^5CGUAm^5CG) in various conformations. The dotted curve is for the random coil or melted (80°C) form. The dashed curve represents a duplex in the B-conformation while the dash-dot curve corresponds to the Z-form duplex. Since actual duplex concentrations were unknown, the spectrum for the melted form were scaled to match the maximum of the deoxynucleoside mix. The B- and Z-form spectra were scaled by the same factor. Although there is residual hypochromism upon melting of long duplexes, there should be little such hypochromism for hexamers. The B-DNA spectrum was recorded in 0.1 mM $MgCl_2$ at pH 7 and 10°C. The B conformation was confirmed by CD measurements. The spectrum of the melted form was obtained simply by raising the temperature to 80°C. The Z-conformer could not be obtained in pure form but only as a mixture with the B-form. The difference spectrum between the B-form and the mixture was used along with known differences between the B and Z forms of poly(m^5CG) to construct the spectrum representing the pure Z-form. The values for the hypochromism of the 260 nm band obtained from these curves are 0.16 and 0.19 for the B- and Z-forms respectively.

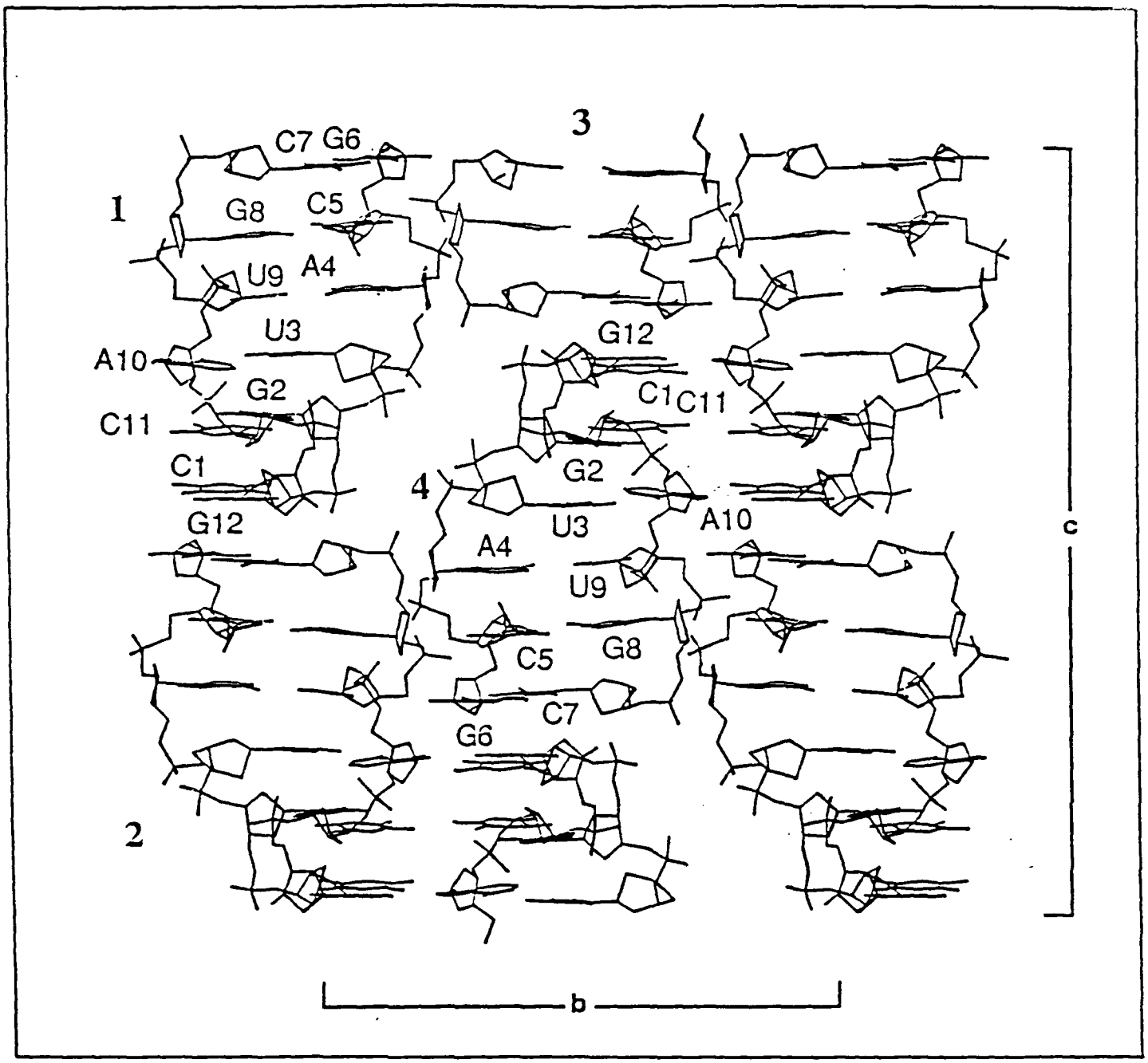
3
C7 G6
1
G8
C5
U9
A4
U3
A10
G2
C11
C1
G12
C1
C11
G2
4
U3
A10
G12
A4
U9
C5
G8
C7
G6
2
c
b

Fig. 1

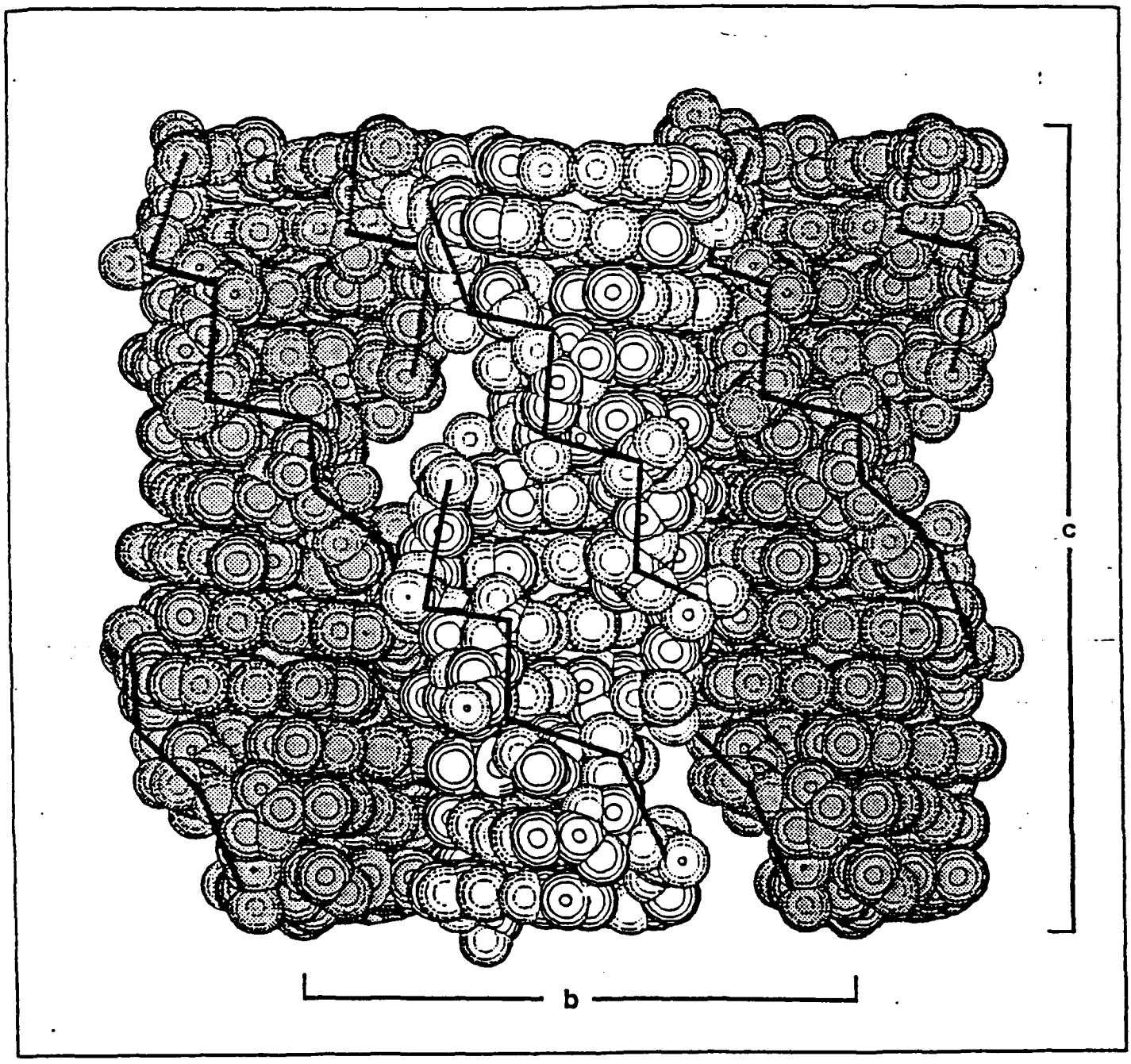

Fig. 2

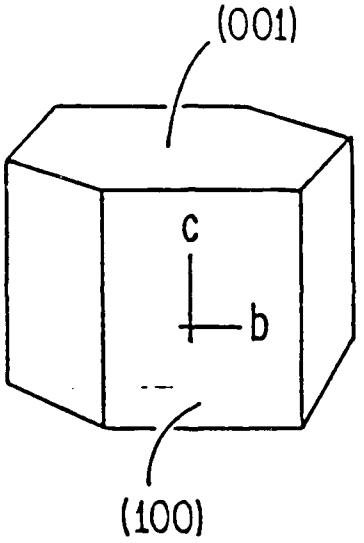

Fig. 3

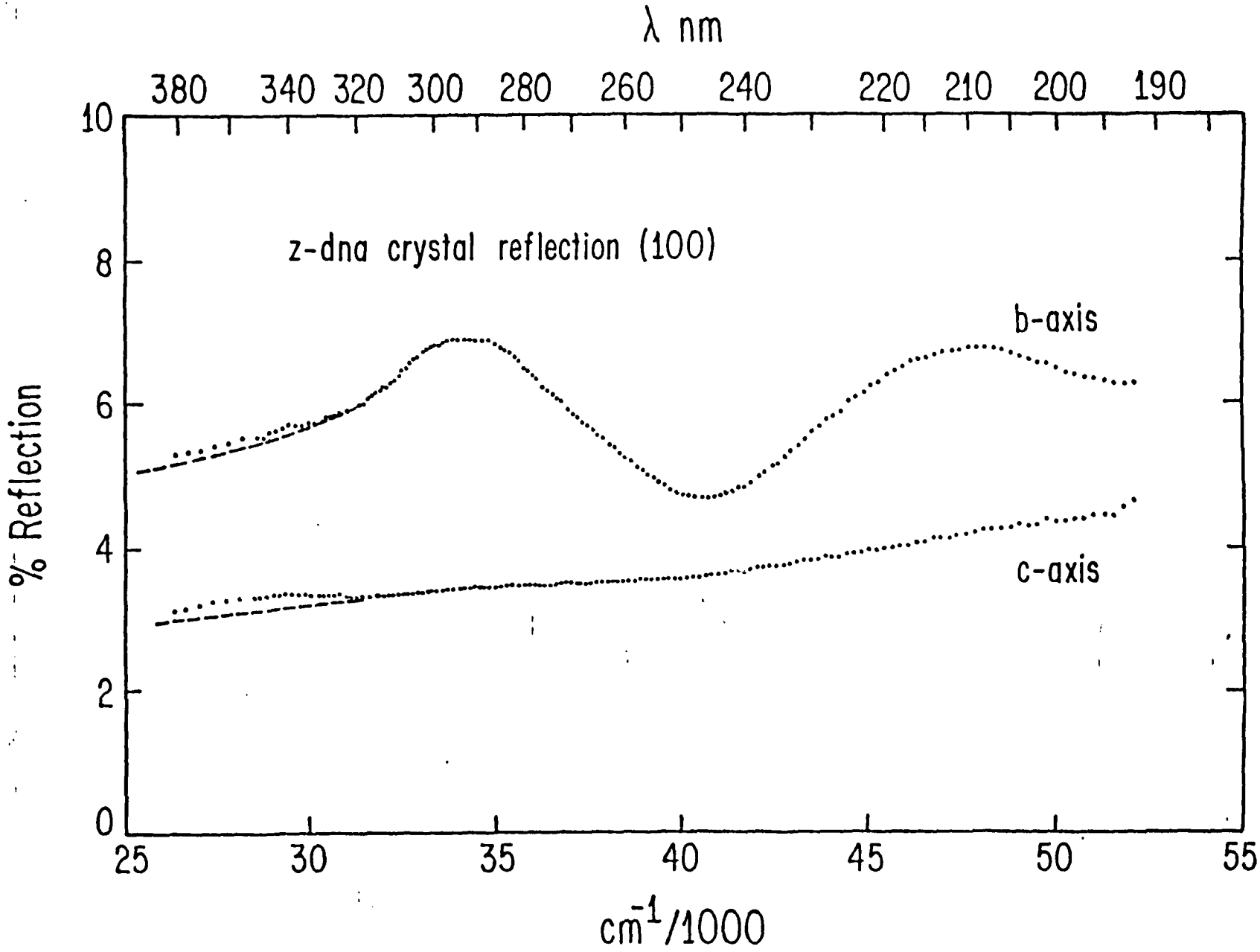
λ nm
380
340
320
300
280
260
240
220
210
200
190
z-dna crystal reflection (100)
b-axis
c-axis
% Reflection
10
8
6
4
2
0
25
30
35
40
45
50
55
cm-1/1000

Fig. 4

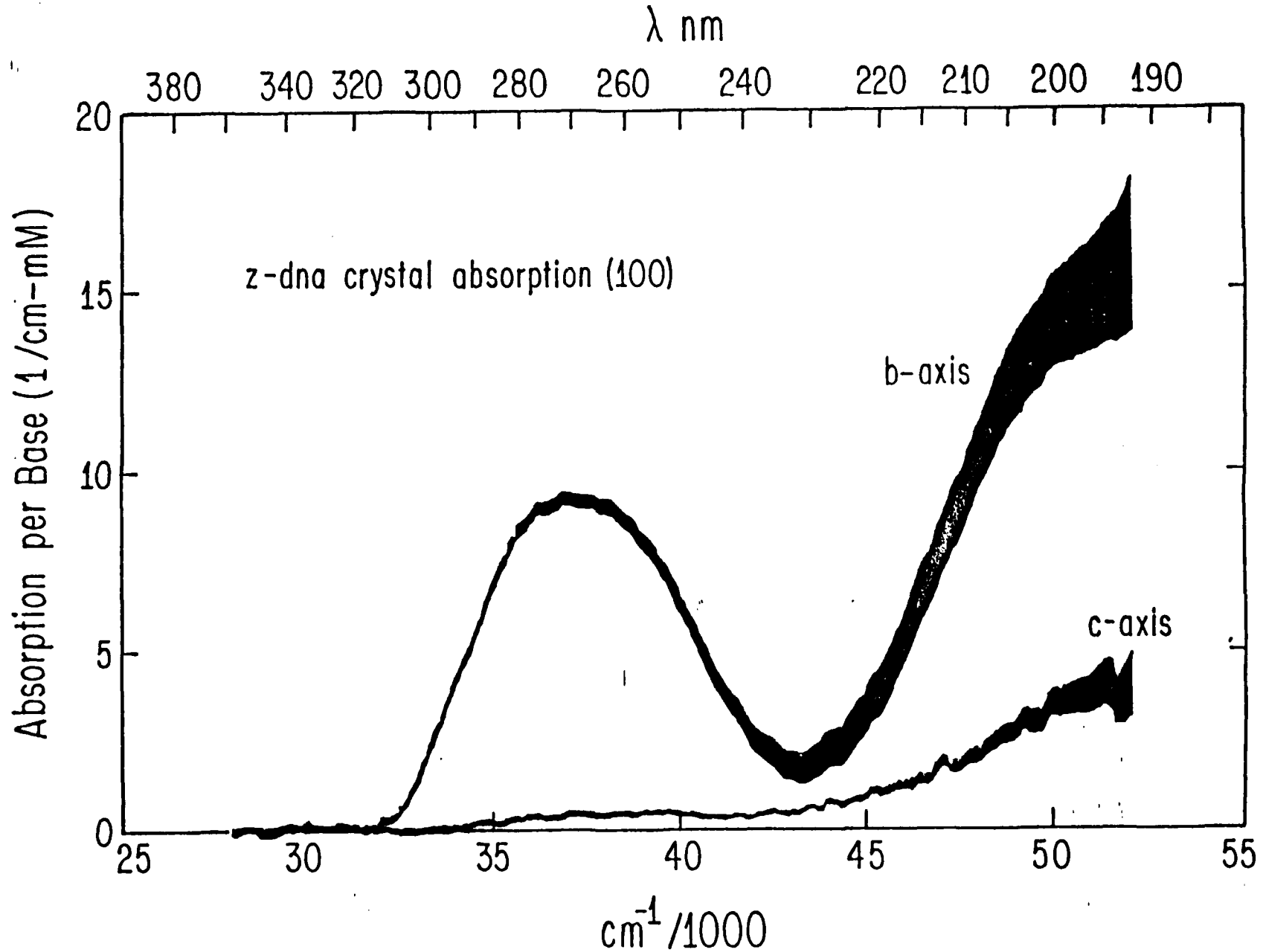
λ nm
380
340
320
300
280
260
240
220
210
200
190
20
15
10
5
0
Absorption per Base (1/cm-mM)
z-dna crystal absorption (100)
b-axis
c-axis
25
30
35
40
45
50
55
cm⁻¹/1000

FIG. 5

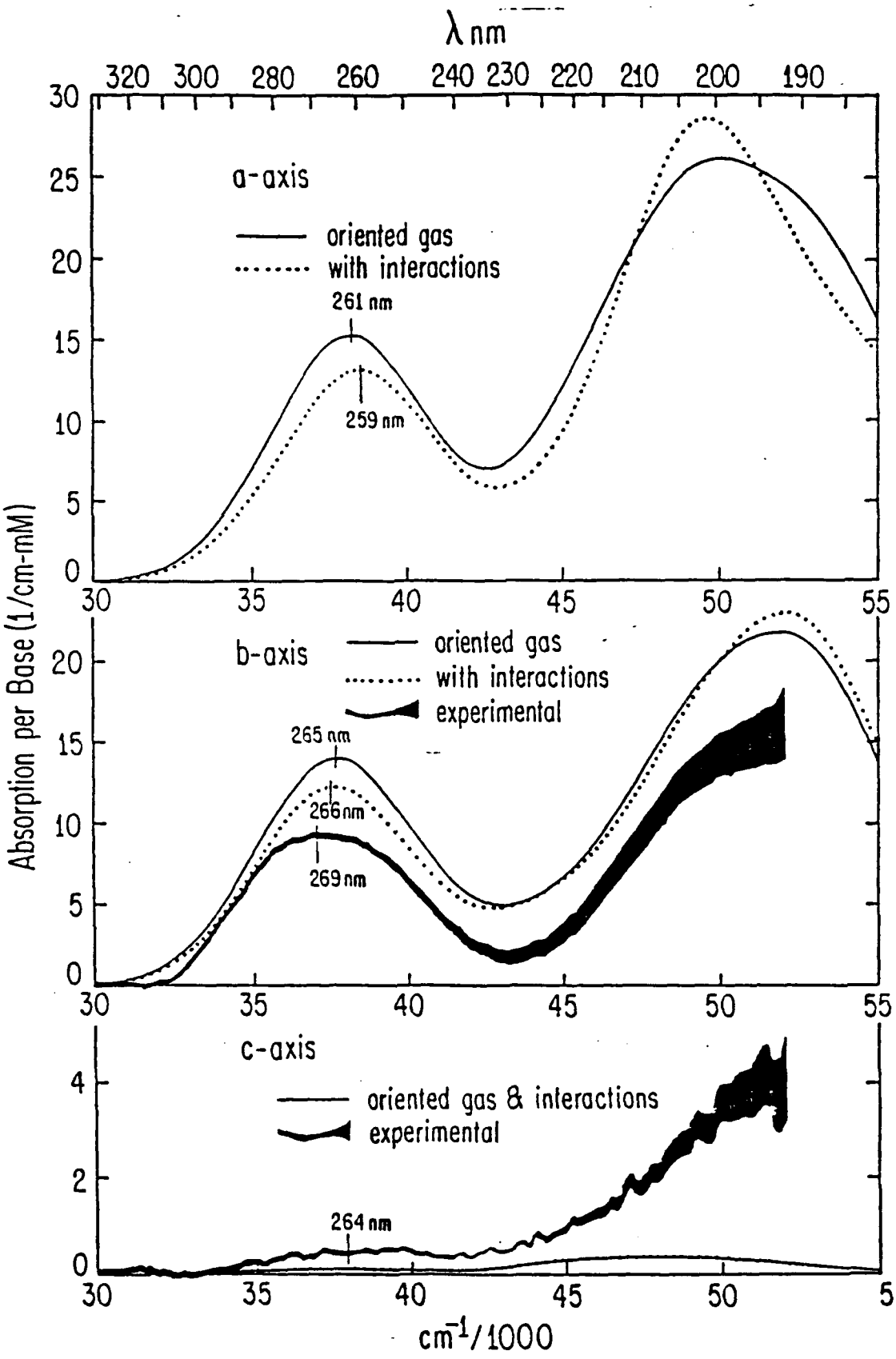
λ nm
320 300 280 260 240 230 220 210 200 190
a-axis
oriented gas
with interactions
261 nm
259 nm
b-axis
oriented gas
with interactions
experimental
265 nm
266 nm
269 nm
c-axis
oriented gas & interactions
experimental
264 nm
Absorption per Base (1/cm-mM)
cm⁻¹/1000

Fig. 6

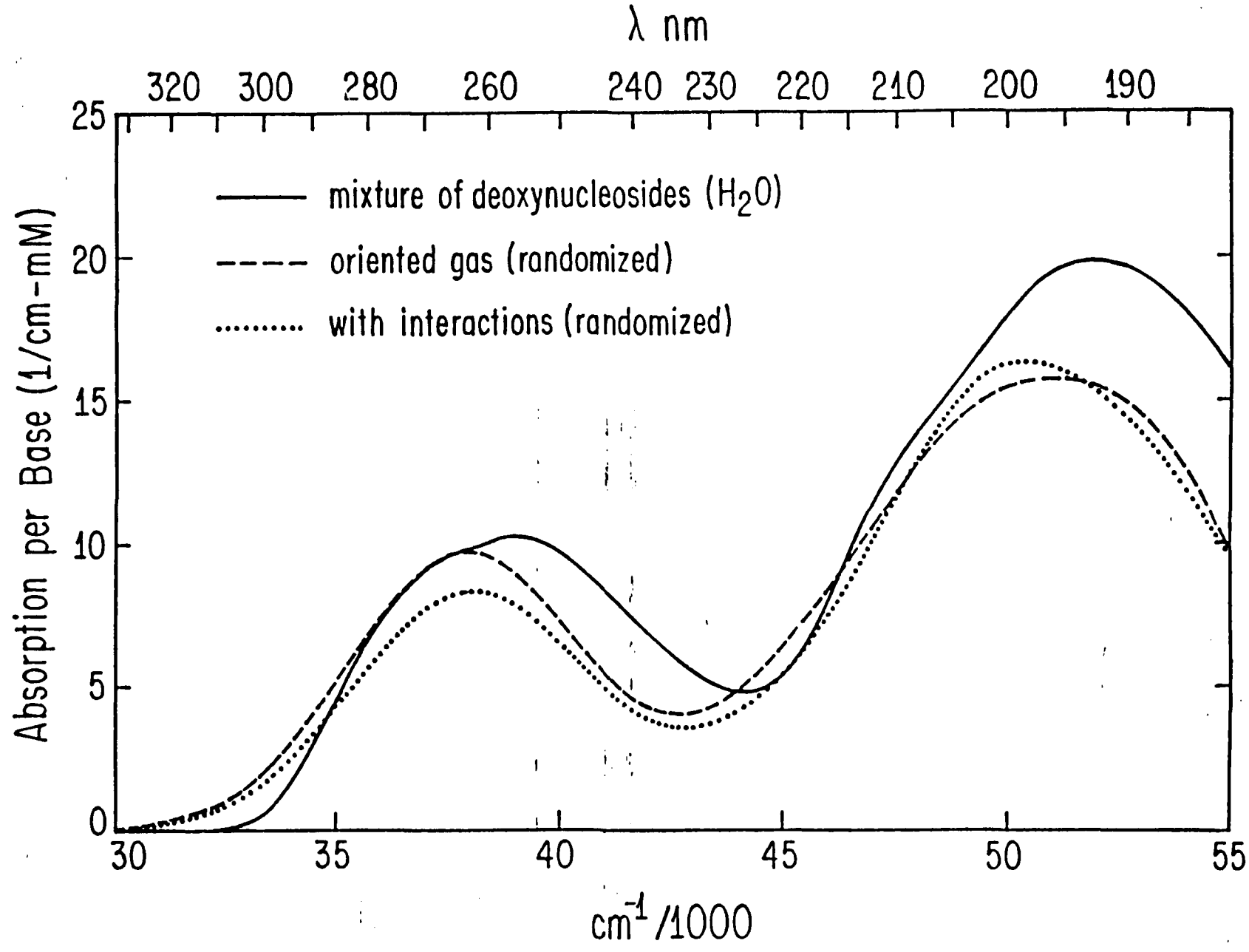
λ nm
320 300 280 260 240 230 220 210 200 190
mixture of deoxynucleosides (H_2O)
oriented gas (randomized)
with interactions (randomized)
Absorption per Base (1/cm-mM)
25
20
15
10
5
0
30 35 40 45 50 55
cm^{-1}/1000

FIG. 7

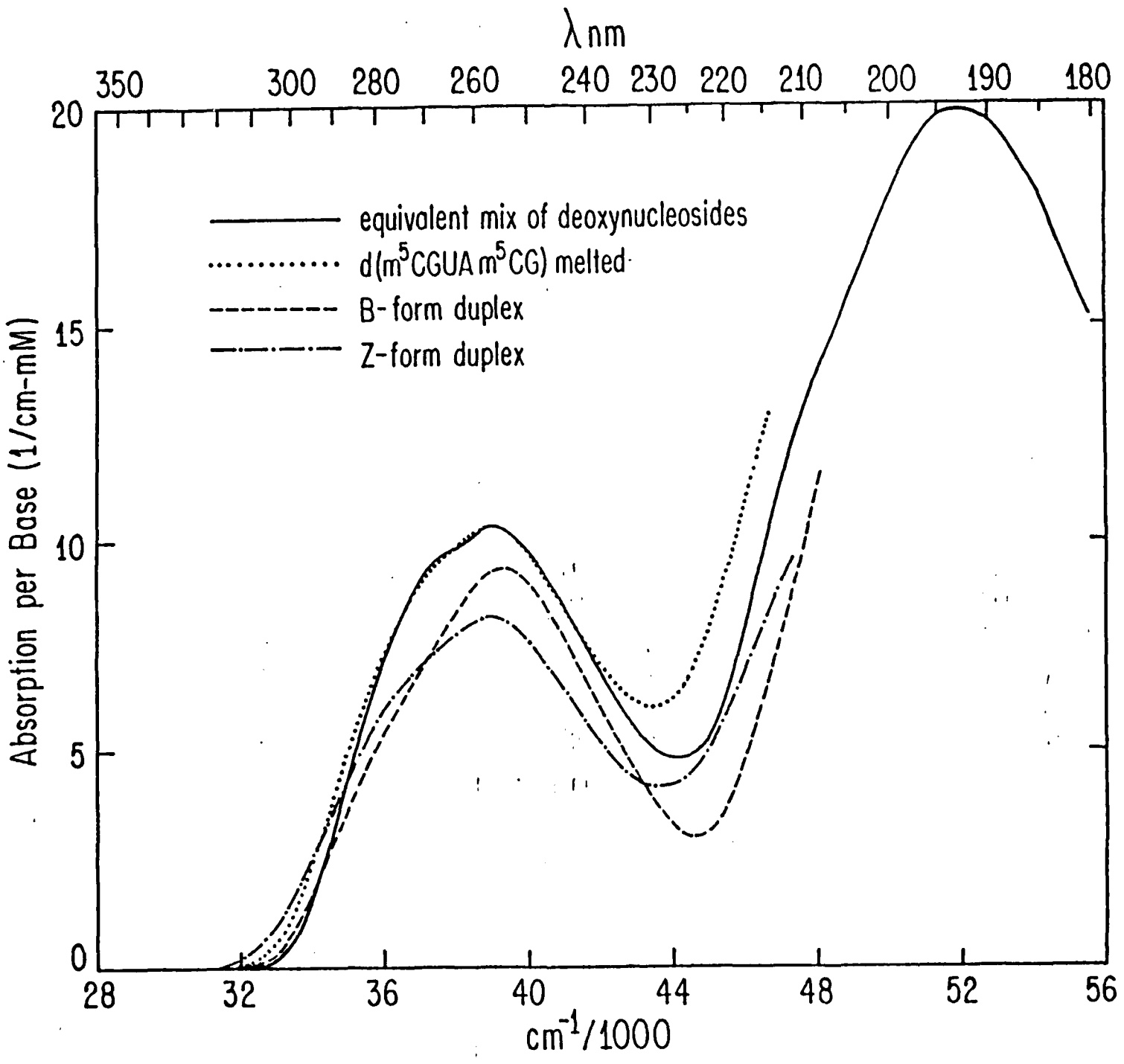
λ nm
350
300
280
260
240
230
220
210
200
190
180
20
15
10
5
0
Absorption per Base (1/cm-mM)
equivalent mix of deoxynucleosides
d(m5CGUA m5CG) melted
B-form duplex
Z-form duplex
28
32
36
40
44
48
52
56
cm-1/1000

FIG. 8